International Journal of High Speed Electronics and Systems
Vol. 13, No. 3 (2003) 873-901

HOT CARRIER EFFECTS WITHIN MACROSCOPIC TRANSPORT MODELS

TIBOR GRASSER
Christian Doppler Laboratory for TCAD in Microelectronics
Institute for Microelectronics, TU Vienna, Gusshausstrasse 27–29
A-1040 Vienna, Austria
Tibor.Grasser@TUWien.ac.at

HANS KOSINA and SIEGFRIED SELBERHERR
Institute for Microelectronics, TU Vienna, Gusshausstrasse 27–29
A-1040 Vienna, Austria

The distribution function of hot carriers in state-of-the-art devices is insufficiently described using just the electric field or the average carrier energy as parameters. Still, the standard models to describe carrier transport in semiconductor devices, namely the drift-diffusion model and the energy-transport model rely on these assumptions. In this article we summarize our work on six moments transport models which allow an accurate characterization of the distribution function. Within this framework it is possible to selfconsistently model the scattering integral without resorting to the relaxation time approximation. In addition, hot electron processes such as impact ionization, which are difficult to model in lower order transport models, can be described accurately.

Keywords: Simulation, semiconductor device modeling, hot carrier effects, moments method, distribution function modeling, numerical analysis

1. Introduction

Accurate modeling of hot carrier effects in modern semiconductor devices has become a crucial ingredient to successful device simulation. In the traditional drift-diffusion model the carrier gas is assumed to be in equilibrium with the electric field[1]. This assumption has been shown to be invalid as the distribution function lags behind the electric field, for both rising and falling fields. In order to obtain information about this non-local behavior of the distribution function, various hydrodynamic and energy-transport models have been proposed[2,3,4]. As a result, it was found that the average carrier energy provides a better basis for modeling physical parameters, like mobility[5,6] and impact ionization[7,8], compared to approaches using the local electric field. In particular, the energy distribution function is commonly modeled using a heated Maxwellian shape[9].

$$f(\mathcal{E}) = A \exp\Big[-\frac{\mathcal{E}}{\mathrm{k_B}\, T_n}\Big] \tag{1}$$

The prefactor A determines the concentration and the carrier temperature T_n is the only parameter to determine the shape of the distribution function. Although the heated Maxwellian approximation provides somewhat more information about the distribution function than is available in the drift-diffusion formalism, it still gives a modest approximation for state-of-the-art devices where the gradients of the electric field are large, as well as for bulk simulations with larger electric fields. In particular, two important effects have been identified:

- In bulk simulations and inside channel regions of MOS transistors, the high energy tail of the distribution function contains fewer carriers than predicted by the heated Maxwellian approximation. This feature of the distribution function has been called the thermal tail[10], because its effective temperature equals the lattice temperature. The overestimation of the number of hot carriers can be significant for modeling hot carrier processes, which relies on this information. In particular, hot carrier processes, such as impact ionization[11] and hot carrier gate currents[12], are significantly overestimated. It was found that the heated Maxwellian approximation provides just a modest extension of the cold Maxwellian approximation, valid only up to approximately 1000 K.
- Inside drain regions of n^+-n-n^+ structures and MOS transistors two carrier populations coexist: the hot carriers coming from the channel mix with the cold carriers residing in the drain region. This mixed distribution shows a significant high energy tail representing the hot carriers of the channel which slowly relax to equilibrium. Because the number of cold carriers is normally significantly larger than the number of hot carriers, the average energy, which determines the slope of the heated Maxwellian distribution, is dominated by the temperature of the cold carriers. Thus the information about the high energy tail is lost in the Maxwellian approximation, which makes it impossible to accurately model hot carrier processes in this regime. However, for instance in the case of impact ionization, hot carriers in that tail still cause a significant number ionization processes.

In recent years it has been shown that the distribution function can be more accurately described when two additional moments are taken into account, resulting in a six moments model[11,13,14,15]. In the following, we review the most important findings in this area and highlight the benefits offered by such a description.

2. Boltzmann's Transport Equation

Transport equations used in semiconductor device simulation are normally derived from Boltzmann's transport equation (BTE), a semi-classical kinetic equation,

which reads[16]

$$\partial_t f + \mathbf{u} \cdot \nabla_{\mathbf{r}} f + \mathbf{F} \cdot \nabla_{\mathbf{p}} f = Q[f] \ , \tag{2}$$

where $f(\mathbf{k}, \mathbf{r}, t)$ represents the carrier distribution function in the six dimensional phase space and the term on the right hand side represents the rate of change of f due to collisions. The BTE is valid for general inhomogeneous materials with arbitrary band structure[17]. To account for quantum effects, equations based on the Wigner-Boltzmann equation have been considered[18]. The group velocity $\mathbf{u}$ is defined as

$$\mathbf{u}(\mathbf{k}, \mathbf{r}) = \nabla_{\mathbf{p}} \mathcal{E}(\mathbf{k}, \mathbf{r}) \ , \tag{3}$$

where $\mathcal{E}$ represents the carrier kinetic energy. The inverse effective mass tensor is defined as

$$\hat{\mathrm{m}}^{-1}(\mathbf{k}, \mathbf{r}) = \nabla_{\mathbf{p}} \otimes \mathbf{u}(\mathbf{k}, \mathbf{r}) = \nabla_{\mathbf{p}} \otimes \nabla_{\mathbf{p}} \mathcal{E}(\mathbf{k}, \mathbf{r}) \ , \tag{4}$$

where $\otimes$ denotes the tensor product[17]. The force $\mathbf{F}$ exerted on the electrons in the presence of electric and magnetic fields and inhomogeneous material properties is generally given as

$$\mathbf{F}(\mathbf{k}, \mathbf{r}) = -\nabla_{\mathbf{r}} \Big(E_{\mathrm{c},0}(\mathbf{r}) + \mathcal{E}(\mathbf{k}, \mathbf{r}) \Big) - \mathrm{q} \Big(\mathbf{E}(\mathbf{r}) + \mathbf{u}(\mathbf{k}, \mathbf{r}) \times \mathbf{B}(\mathbf{r}) \Big) \tag{5}$$

and depends on both $\mathbf{k}$ and $\mathbf{r}$. The two spatial gradients ($\nabla_{\mathbf{r}}$) account for changes in the bottom of the conduction band edge $E_{\mathrm{c},0}$ and the shape of the band structure. Omitting the influence of the magnetic field and assuming homogeneous materials, $\mathbf{F}$ simplifies to the electrostatic force

$$\mathbf{F}(\mathbf{r}) = -\mathrm{q}\mathbf{E}(\mathbf{r}) \ . \tag{6}$$

In the following, we will only consider position-independent masses, but permit energy-dependent masses.

The BTE represents an integro-differential equation in the seven-dimensional space $(\mathbf{k}, \mathbf{r}, t)$. To solve this equation numerically by discretization of the differential and integral operators is computationally very expensive. A widely used numerical method for solving the BTE is the Monte Carlo (MC) method. This method has been proven to give accurate results, but is still computationally expensive. Furthermore, if the distribution of high-energetic carriers is relevant, or if the carrier concentration is very low in specific regions of the device, MC simulations tend to produce high variance in the results. Another approach, which is based on an expansion of the distribution function in momentum space into a series of spherical harmonics, has been successfully used to solve the BTE[19,20]. In contrast to the MC method, the spherical harmonic expansion method is deterministic and the computational effort, while still high, is significantly reduced. However, by only considering the lower order terms of the expansion, approximations are introduced

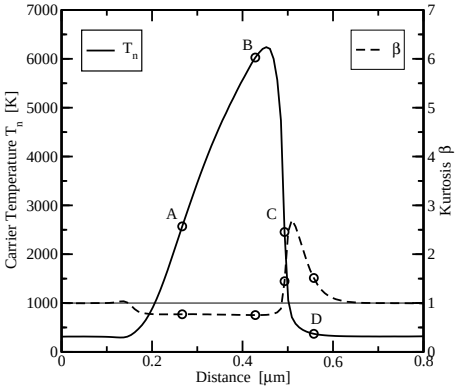

Fig. 1. Electron temperature inside an n^+-n-n^+ structure with $L_C = 200$ nm. Also shown is the normalized fourth-order moment β, which indicates the deviation from the Maxwellian shape.

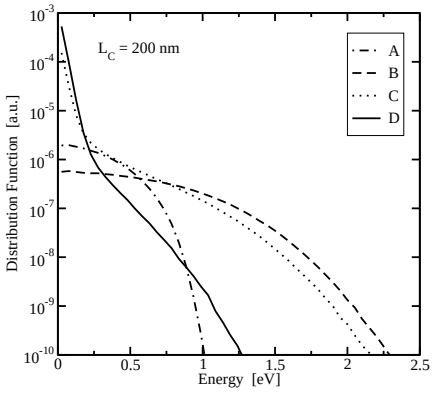

Fig. 2. The distribution function at the four characteristic points. The average energies at the points A and C are the same, whereas the distribution function looks completely different. At point D, where the carrier temperature is 370 K, a significant high-energy tail exists.

whose influence on the accuracy of the simulation results is still not fully clarified. Particularly in the ballistic regime numerically calculated full-band structures cannot be included, as opposed to the MC method, where usage of such band structures is a solved problem.

A common simplification is to investigate only a few moments of the distribution function, such as the carrier concentration and the carrier temperature. A moment is obtained by multiplying the distribution function with a suitable weight function $\phi = \phi(\mathbf{k})$ and integrating over $\mathbf{k}$-space.

$$\langle \phi(\mathbf{k}) \rangle = \frac{1}{n} \int \phi(\mathbf{k}) f(\mathbf{k}) \, \mathrm{d}^3\mathbf{k} \qquad \text{with} \quad n = \int f(\mathbf{k}) \, \mathrm{d}^3\mathbf{k} \tag{7}$$

Thus, the three k-coordinates are eliminated at the expense of information loss concerning the details of the distribution function.

One of the fundamental problems of energy-transport models is that only the average energy is available to characterize the distribution function. Therefore, a heated Maxwellian distribution is frequently assumed for the closure of the equation system and for modeling various physical processes. This assumption is significantly violated in modern semiconductor devices. Monte Carlo simulation results of an n^+-n-n^+ structure with a channel length of $L_C = 200$ nm are shown in Fig. 1 and Fig. 2. Even though the average energy is the same at points A and C, the distribution function looks completely different in both cases[21,22]. A heated Maxwellian distribution, which gives a straight line in a semi-logarithmic plot, is definitely a poor approximation throughout the whole device.

Additional information is obtained by including the fourth- and fifth-order moment of the distribution function which results in a six moments transport model.

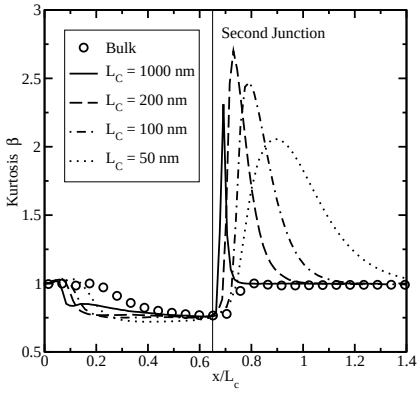

Fig. 3. The kurtosis of different n^+-n-n^+ structures. Note the strong deviation from unity after the second junction.

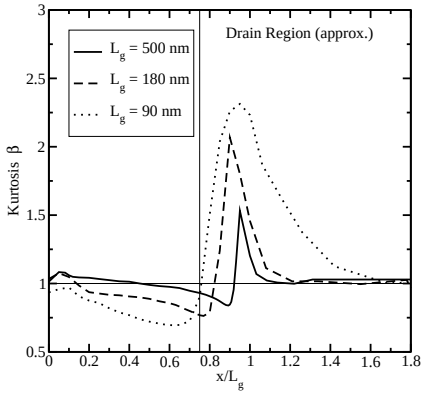

Fig. 4. The kurtosis of different MOS transistors. Note the strong deviation from unity in the drain region.

We define the kurtosis of the distribution function by normalizing the fourth-order moment $\langle \mathcal{E}^2 \rangle$ to give

$$\beta = \frac{3}{5} \frac{\langle \mathcal{E}^2 \rangle}{\langle \mathcal{E} \rangle^2} \ , \tag{8}$$

which is also shown in Fig. 1. For a heated Maxwellian distribution and parabolic bands $\beta = \beta_{\mathrm{MB}} = 1$. Thus the deviation of β from unity quantifies the deviation from the Maxwellian shape in the parabolic case. When non-parabolic bands are taken into account, the value of β_{MB} depends on the mean energy but stays close to unity. Note, however, that a Maxwellian shape is never observed in Monte Carlo simulations, except for the contact regions where the carriers are still in equilibrium.

Typical values of the kurtosis β are in the range [0.75, 3] which indicates a strong deviation from a heated Maxwellian distribution. In addition, as shown in Fig. 3, the kurtosis behaves fundamentally different than in bulk where a unique relationship $\beta_{\mathrm{Bulk}}(T_n)$ exists[15]. Especially at the drain side of the structures we observe a strong deviation from the Maxwellian case and even from the bulk non-Maxwellian case. This deviation corresponds to the high-energy tail in Fig. 2 and can be used to reconstruct the distribution function from the moments.

3. Band Structure

For the formulation of transport models, a description of the band structure $\mathcal{E}(\mathbf{k})$ is required. The band structure of semiconductors is in general very complex and several simplifications are required to obtain tractable macroscopic transport models. Firstly, it is usually assumed that the band structure is isotropic, that is, the kinetic energy depends only on the magnitude of the wave vector $\mathbf{k}$. With this assumption

the dispersion relation can be written in terms of the band form function γ

$$\gamma(\mathcal{E}) = \frac{\mathbf{p}^2}{2m^*} = \frac{\hbar^2 k^2}{2m^*} \ . \tag{9}$$

The simplest approximation for the real band structure is a parabolic relationship between the energy and the carrier momentum $\hbar\mathbf{k}$,

$$\gamma(\mathcal{E}) = \mathcal{E} \ , \tag{10}$$

which is assumed to be valid for energies close to the band minimum. A first order non-parabolic relationship was given by Kane[23],

$$\gamma(\mathcal{E}) = \mathcal{E}(1+\alpha\mathcal{E}) = \mathcal{E}H_{\mathcal{E}}(\alpha\mathcal{E}) \ , \tag{11}$$

with α being the non-parabolicity correction factor. Kane's dispersion relation results in the following relationship between momentum and velocity

$$\mathbf{u} = \frac{\hbar\mathbf{k}}{m^*}\frac{1}{1+2\alpha\mathcal{E}} = \frac{\hbar\mathbf{k}}{m^*}\sum_{i=0}^{\infty}(-2\alpha\mathcal{E})^i = \frac{\hbar\mathbf{k}}{m^*}H_{\mathrm{u}}(\alpha\mathcal{E}) \ . \tag{12}$$

The series expansion shows that the average velocity will contain an infinite number of higher order moments which are not necessarily negligible. This is problematic because these quantities are additional unknowns which prohibits closed form solutions.

To obtain a more tractable expression Cassi and Riccò[24] approximated Kane's dispersion relation as

$$\gamma(\mathcal{E}) = x\mathcal{E}^y \tag{13}$$

and fitted the parameters x and y for different energy ranges. For $y = 1$ the conventional parabolic dispersion relation is obtained. However, the resulting density of states shows a "parabolic-like" behavior and is therefore of limited value for the description of non-parabolic transport phenomena[15]. To include "non-parabolic-like" behavior without loosing accuracy in the low-energy region we have proposed to use the density of states[15]

$$g(\mathcal{E}) = g_0\sqrt{\mathcal{E}}\Big(1+\gamma_{\mathrm{g}}(\alpha\mathcal{E})^{\lambda_{\mathrm{g}}}\Big) \ . \tag{14}$$

4. Boltzmann's Equation and the Diffusion Approximation

Macroscopic transport models derived from the BTE contain so-called convective terms which make the handling of the resulting equations cumbersome. Thus additional simplifications are required to obtain manageable transport models. Several

simplifications can be formally justified by considering the diffusion limit of Boltzmann's equation which will be explained in the following. We continue with the scaled form of the BTE[25]

$$\kappa\,\partial_t f + \mathbf{u}\cdot\nabla_{\mathbf{r}} f + \mathbf{F}\cdot\nabla_{\mathbf{p}} f = \frac{1}{\kappa}\,Q[f]\ . \tag{15}$$

The Knudsen number κ appears as a scaling parameter which represents the mean free path $\tau_0 v_0$ relative to the device dimension[25].

$$\kappa = \frac{\tau_0 v_0}{x_0} \tag{16}$$

Here, τ_0 is the characteristic time between scattering events, v_0 denotes the velocity scale and x_0 is given by the size of the simulation domain. Carriers in a semiconductor at room temperature are frequently considered a collision-dominated system, for which $\kappa \ll 1$. Diffusion scaling assumes the time scale of the system to be

$$t_0 = \frac{\tau_0}{\kappa^2}\ . \tag{17}$$

For both the macroscopic transport models and the modeling of the distribution function it is advantageous to split the distribution function into its symmetric and anti-symmetric parts as

$$f(\mathbf{k}) = f_{\mathrm{S}}(\mathbf{k}) + \kappa f_{\mathrm{A}}(\mathbf{k})\ . \tag{18}$$

This is because only the symmetric part $f_{\mathrm{S}}(\mathbf{k})$ contributes to averages with the even weight functions whereas the anti-symmetric part $f_{\mathrm{A}}(\mathbf{k})$ contributes to the averages related to odd weight functions. Without loss of generality, the symmetric and anti-symmetric parts of the distribution function $f(\mathbf{k})$ are obtained via the following relations

$$f_{\mathrm{S}}(\mathbf{k}) = \tfrac{1}{2}\left(f(\mathbf{k}) + f(-\mathbf{k})\right)\ , \tag{19}$$

$$\kappa f_{\mathrm{A}}(\mathbf{k}) = \tfrac{1}{2}\left(f(\mathbf{k}) - f(-\mathbf{k})\right)\ . \tag{20}$$

By inserting (18) into (15) Boltzmann's equation splits into two equations

$$\partial_t f_{\mathrm{S}} + \mathbf{u}\cdot\nabla_{\mathbf{r}} f_{\mathrm{A}} + \mathbf{F}\cdot\nabla_{\mathbf{p}} f_{\mathrm{A}} = \frac{1}{\kappa^2}\,Q_{\mathrm{S}}[f_{\mathrm{S}}]\ , \tag{21}$$

$$\kappa^2\,\partial_t f_{\mathrm{A}} + \mathbf{u}\cdot\nabla_{\mathbf{r}} f_{\mathrm{S}} + \mathbf{F}\cdot\nabla_{\mathbf{p}} f_{\mathrm{S}} = Q_{\mathrm{A}}[f_{\mathrm{A}}]\ . \tag{22}$$

So far no simplifications have been introduced and (21) and (22) are equivalent to (15). We now assume that the system is diffusion dominated, that is $\kappa \ll 1$, and neglect all terms of order $O(\kappa^2)$. This assumption is known as the *diffusion approximation*[25] and we obtain

$$\partial_t f_{\mathrm{S}} + \mathbf{u}\cdot\nabla_{\mathbf{r}} f_{\mathrm{A}} + \mathbf{F}\cdot\nabla_{\mathbf{p}} f_{\mathrm{A}} = \frac{1}{\kappa^2}\,Q_{\mathrm{S}}[f_{\mathrm{S}}]\ , \tag{23}$$

$$\mathbf{u}\cdot\nabla_{\mathbf{r}} f_{\mathrm{S}} + \mathbf{F}\cdot\nabla_{\mathbf{p}} f_{\mathrm{S}} = Q_{\mathrm{A}}[f_{\mathrm{A}}]\ . \tag{24}$$

In addition we can derive a relationship between the symmetric and anti-symmetric parts when we assume that $f(\mathbf{k})$ can be obtained by displacing a symmetric function $f_{\mathrm{S}}(\mathbf{k})$ by $\kappa\,\mathbf{k}_0$. Under the assumption that $f_{\mathrm{S}}(\mathbf{k})$ is isotropic, that is, it depends only on the modulus of $\mathbf{k}$ and that $\kappa\,\mathbf{k}_0$ is small we expand the distribution function

$$f(\mathbf{k}) = f_{\mathrm{S}}(\mathbf{k} - \kappa\,\mathbf{k}_0) \approx f_{\mathrm{S}}(\mathbf{k}) - \partial_\kappa f(\mathbf{k}) \cdot \kappa\,\mathbf{k}_0 \tag{25}$$

and neglect all terms of order $O(\kappa^2)$, consistently with the diffusion approximation.

4.1. *Displaced and Heated Maxwellian Approximation*

To illustrate the consequences of the diffusion approximation we consider a Maxwellian distribution function

$$f_{\mathrm{M}}(\mathbf{k}) = f_{\mathrm{M}}(k) = A\,\exp\Big[-\frac{\mathbf{k}^2}{a_k}\Big] \tag{26}$$

which is displaced by $\kappa\,\mathbf{k}_0$ to give

$$f(\mathbf{k}) = f_{\mathrm{M}}(\mathbf{k} - \kappa\,\mathbf{k}_0) = A\,\exp\Big[-\frac{(\mathbf{k} - \kappa\,\mathbf{k}_0)^2}{a_k}\Big]\ . \tag{27}$$

For the symmetric and anti-symmetric parts we obtain

$$f_{\mathrm{S}}(\mathbf{k}) = f_{\mathrm{M}}(\mathbf{k}) \exp\Big[-\frac{\kappa^2\,\mathbf{k}_0^2}{a_k}\Big] \cosh\Big[\frac{2}{a_k}\kappa\,\mathbf{k}_0 \cdot \mathbf{k}\Big]\ , \tag{28}$$

$$f_{\mathrm{A}}(\mathbf{k}) = f_{\mathrm{M}}(\mathbf{k}) \exp\Big[-\frac{\kappa^2\,\mathbf{k}_0^2}{a_k}\Big] \sinh\Big[\frac{2}{a_k}\kappa\,\mathbf{k}_0 \cdot \mathbf{k}\Big]\ . \tag{29}$$

Assuming that κ is small we obtain from (25)

$$f_{\mathrm{S}}(\mathbf{k}) = f_{\mathrm{M}}(\mathbf{k}) \tag{30}$$

$$f_{\mathrm{A}}(\mathbf{k}) = -\partial_\kappa f(\mathbf{k}) \cdot \kappa\,\mathbf{k}_0 = f_{\mathrm{M}}(\mathbf{k})\,\frac{2}{a_k}\mathbf{k} \cdot \kappa\,\mathbf{k}_0 \tag{31}$$

for the symmetric and anti-symmetric part. The impact of this approximation is shown in Fig. 5 for a small and a large displacement, respectively. Whereas for a small displacement the accuracy is good, the characteristic double-humps are removed for larger displacements.

4.2. *Influence on Transport Equations*

The framework of the diffusion approximation allows one to considerably simplify the structure of the transport equations. To point out the implications of the diffusion approximation the important moments resulting from the weight functions $\mathbf{k} \cdot \mathbf{k}$ and $\mathbf{k} \otimes \mathbf{k}$, which cause the aforementioned complications, are evaluated in this section without applying the diffusion approximation. Let $f(\mathbf{k})$ be a displaced distribution function

$$f(\mathbf{k}) = f_0(\mathbf{k} - \kappa\,\mathbf{k}_0)\ , \tag{32}$$

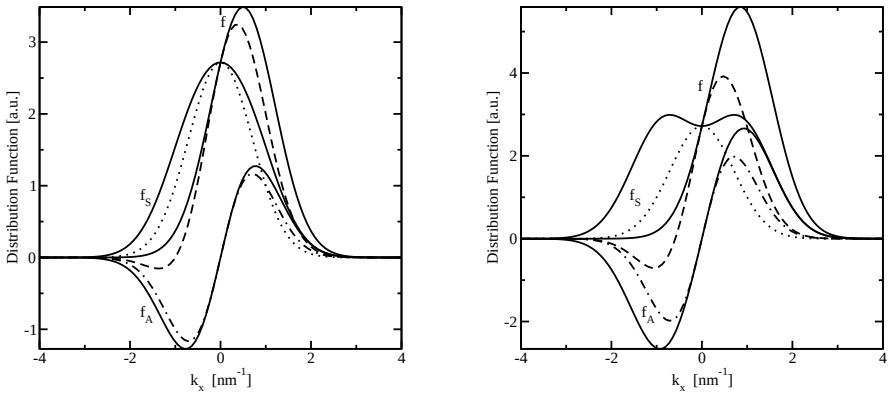

Fig. 5. Shape of a displaced Maxwell distribution function and its symmetric $f_{\mathrm{S}}(k)$ and anti-symmetric $f_{\mathrm{A}}(k)$ parts. The displacement is assumed to be small (left) and large (right). The solid lines give the exact solution, whereas the diffusion approximation is represented by the other linestyles.

where f_0 is not only symmetric in $\mathbf{k}$ but also in every component of $\mathbf{k}$

$$f_0(k_x, k_y, k_z) = f_0(-k_x, k_y, k_z) = f_0(k_x, -k_y, k_z) = f_0(k_x, k_y, -k_z) \ . \tag{33}$$

This stronger symmetry property ensures that the resulting tensor quantities are of diagonal shape. Although off-diagonal elements are usually neglected anyway, the symmetry requirement (33) gives the formal justification of this approximation. Functions which satisfy this stronger symmetry criterion are for example isotropic distribution functions where $f_0(\mathbf{k})$ is only a function of the absolute value of $\mathbf{k}$, $f_0(\mathbf{k}) = f_0(|\mathbf{k}|)$, and whose iso-surfaces are spheres. Another example is a distribution with ellipsoidal iso-surfaces, for instance an anisotropic Maxwell distribution[26].

Without loss of generality we split $f(\mathbf{k})$ into its symmetric and anti-symmetric parts. Since the weight functions $\mathbf{k} \cdot \mathbf{k}$ and $\mathbf{k} \otimes \mathbf{k}$ are even functions, only the symmetric part of the distribution function has to be taken into account

$$f_{\mathrm{S}}(\mathbf{k}) = \tfrac{1}{2} \left(f_0(\mathbf{k} - \kappa\, \mathbf{k}_0) + f_0(\mathbf{k} + \kappa\, \mathbf{k}_0) \right) \ . \tag{34}$$

Equation (34) is now used in the evaluation of the statistical average $\langle \mathbf{k} \otimes \mathbf{k} \rangle$:

$$n \langle \mathbf{k} \otimes \mathbf{k} \rangle = \int \mathbf{k} \otimes \mathbf{k}\, f_{\mathrm{S}}(\mathbf{k})\ \mathrm{d}^3\mathbf{k} = \int \mathbf{k} \otimes \mathbf{k}\, f_0(\mathbf{k})\ \mathrm{d}^3\mathbf{k} + \kappa^2\, \mathbf{k}_0 \otimes \mathbf{k}_0\, n \ . \tag{35}$$

The statistical average of $\langle \mathbf{k} \cdot \mathbf{k} \rangle$ can be evaluated in the same way yielding

$$n \langle \mathbf{k} \cdot \mathbf{k} \rangle = \int \mathbf{k} \cdot \mathbf{k}\, f_0(\mathbf{k})\ \mathrm{d}^3\mathbf{k} + \kappa^2\, \mathbf{k}_0 \cdot \mathbf{k}_0\, n \ . \tag{36}$$

In the diffusion limit ($\kappa \ll 1$) one thus acquires that convective terms of the form $\langle \mathbf{k} \rangle \otimes \langle \mathbf{k} \rangle$ and $\langle \mathbf{k} \rangle \cdot \langle \mathbf{k} \rangle$ are neglected against terms of the form $\langle \mathbf{k} \otimes \mathbf{k} \rangle$ and $\langle \mathbf{k} \cdot \mathbf{k} \rangle$,

respectively. One of the consequences is that the drift kinetic energy $m^*\langle \mathbf{u} \rangle^2/2$ is neglected against the thermal energy $\mathrm{k_B}T_n$.

The diffusion approximation thus provides a formal framework which justifies the transition from hydrodynamic models to energy-transport models. Note that this simplification is necessary to obtain an equation system suitable for engineering applications. The otherwise obtained hydrodynamic equations are similar to the hyperbolic Euler equations of fluid dynamics with the addition of a heat conduction term and the collision terms[27]. They describe the propagation of electrons in a semiconductor device as the flow of a compressible, charged fluid. This electron gas has a sound speed, and the electron flow may be either subsonic or supersonic. In the case of supersonic flow electron shock waves will in general develop inside the device[28]. These shock waves occur at either short length-scales or at low temperatures. As the equation system is hyperbolic in the supersonic regions, special numerical methods have to be used which are not compatible to the methods employed for the parabolic convection-diffusion type of equations. Although much effort has been put into the investigation of hydrodynamic models, the equations remain extremely difficult to handle and are as such not used under practical circumstances[4].

5. Distribution Function Model

We will now give models for the symmetric and anti-symmetric parts of the distribution function within the framework of the diffusion approximation.

5.1. *Symmetric Part*

The symmetric part is modeled according to our previous works[15] as consisting of a hot (f_h) and a cold distribution (f_c).

$$f_\mathrm{S}(\mathcal{E}) = A\Big\{\exp\Big[-\Big(\frac{\mathcal{E}}{a}\Big)^b\Big] + c\exp\Big[-\frac{\mathcal{E}}{a_\mathrm{c}}\Big]\Big\} \tag{37}$$

$$= A\Big\{f_\mathrm{h}(\mathcal{E}) + c\, f_\mathrm{c}(\mathcal{E})\Big\} \tag{38}$$

The five parameters A, a, b, c, and a_c, are calculated in such a way that f_S exactly reproduces the first three even moments provided by the six moments model. We calculate the even moments of the distribution function using the weight functions

$$\phi_i = \mathcal{E}^i \tag{39}$$

to obtain

$$\langle \phi_i \rangle = \frac{1}{n}\int \phi_i\, f_\mathrm{S}(\mathcal{E})\ \mathrm{d}^3\mathbf{k} \qquad i = 0, 1, 2\ . \tag{40}$$

Note that the moments of ϕ_i depend only on the symmetric part of the distribution function. In addition, the conditions $a_\mathrm{c} = \mathrm{k_B}T_\mathrm{L}$ and $\langle \mathcal{E}^2 \rangle_\mathrm{h} = h(\langle \mathcal{E} \rangle_\mathrm{h})$ are assumed, where $h(\langle \mathcal{E} \rangle)$ is the relationship between $\langle \mathcal{E}^2 \rangle$ and $\langle \mathcal{E} \rangle$ in bulk, and $\langle \cdot \rangle_\mathrm{h}$ is the moment

of f_{h} only. Note that the cold population only exists inside the drain regions and that therefore c vanishes inside channel regions[15]. Introducing the auxiliary functions

$$\mathcal{G}(x,a,b) = \frac{a^{x+\frac{3}{2}}}{b}\Gamma\Big(\frac{x+\frac{3}{2}}{b}\Big) \;, \tag{41}$$

$$\mathcal{I}_{\mathrm{y}}(x,a,b) = \mathcal{G}(x,a,b) + \gamma_{\mathrm{y}}\alpha^{\lambda_{\mathrm{y}}}\,\mathcal{G}(x+\lambda_{\mathrm{y}},a,b) \;, \tag{42}$$

$$m_{\mathrm{y}}(x) = \mathcal{I}_{\mathrm{y}}(x,a,b) + c\,\mathcal{I}_{\mathrm{y}}(x,a_{\mathrm{c}},1) \;, \tag{43}$$

and $C_{\mathrm{m}} = A\,g_0$ we obtain

$$n = C_{\mathrm{m}} m_{\mathrm{g}}(0) \qquad \text{and} \qquad \langle\phi_i\rangle = \frac{m_{\mathrm{g}}(i)}{m_{\mathrm{g}}(0)} \;, \tag{44}$$

with $m_{\mathrm{y}}(x)$ being the generalized moment of $f_{\mathrm{S}}(\mathcal{E})$ using the parameters γ_{y} and λ_{y}.

Thus the following algebraic nonlinear equation system for (a,b,c) is solved using Newton's method

$$\Big(\frac{m_{\mathrm{g}}(1)}{m_{\mathrm{g}}(0)}, \frac{m_{\mathrm{g}}(2)}{m_{\mathrm{g}}(0)}, \frac{\mathcal{I}_{\mathrm{y}}(2,a_{\mathrm{c}},1)}{\mathcal{I}_{\mathrm{y}}(0,a_{\mathrm{c}},1)}\Big) = \Big(\langle\mathcal{E}\rangle, \langle\mathcal{E}^2\rangle, h\Big(\frac{\mathcal{I}_{\mathrm{y}}(1,a_{\mathrm{c}},1)}{\mathcal{I}_{\mathrm{y}}(0,a_{\mathrm{c}},1)}\Big)\Big) \;. \tag{45}$$

Note that $\langle\mathcal{E}\rangle$ and $\langle\mathcal{E}^2\rangle$ are obtained from the solution of the six moments model. As stated above, in the drain region $c = 0$ is assumed and the last equation of (45) is dropped.

5.2. *Anti-Symmetric Part*

The anti-symmetric part is obtained by displacing the symmetric part by

$$\mathbf{k}_{\mathrm{c}} = \sum_{j=0}^{2} \mathcal{E}^j \mathbf{k}_j \cdot \mathbf{k} \tag{46}$$

and applying the diffusion approximation

$$f_{\mathrm{A}}(\mathbf{k}) = \sum_{j=0}^{2} \mathcal{E}^j \mathbf{B}_j \cdot \mathbf{k}\, f_{\mathcal{E}}(\mathcal{E}) \;, \tag{47}$$

with $f_{\mathcal{E}}(\mathcal{E}) = f_{\mathrm{h}}(\mathcal{E}) + c_{\mathrm{A}}\, f_{\mathrm{c}}(\mathcal{E})$. Note that a different prefactor appears in front of f_{c} because the cold electron gas has a different average energy and velocity. This prefactor is empirically modeled as $c_{\mathrm{A}}/c = a_{\mathrm{c}}/a$.

To determine the coefficients $\mathbf{B}_i$ we calculate the moments of the anti-symmetric part of the distribution function using the weight functions

$$\Phi_i^{\mathbf{u}} = \mathbf{u}\mathcal{E}^i = \frac{\hbar\mathbf{k}}{m^*}\mathcal{E}^i H_{\mathrm{u}}(\alpha\mathcal{E}) \tag{48}$$

and require that they exactly reproduce the three fluxes occuring in the six moments model. The expressions for the moments are

$$\langle \Phi_i^{\mathbf{u}} \rangle = \frac{\hbar}{m^* n} \sum_{j=0}^{2} \mathbf{B}_j \int \mathcal{E}^{i+j} (\mathbf{k} \otimes \mathbf{k}) H_{\mathrm{u}}(\alpha\mathcal{E}) f_{\mathcal{E}}(\mathcal{E}) \, \mathrm{d}^3\mathbf{k} \tag{49}$$

$$= C_{\mathrm{M}} \sum_{j=0}^{2} \mathbf{B}_j \int \mathcal{E}^{i+j+3/2} H_{\mathrm{M}}(\alpha\mathcal{E}) f_{\mathcal{E}}(\mathcal{E}) \, \mathrm{d}\mathcal{E} \ . \tag{50}$$

Here we introduced $C_{\mathrm{M}} = 2g_0/(3\hbar n)$ and

$$H_{\mathrm{g}}(\alpha\mathcal{E}) = \sqrt{1+\alpha\mathcal{E}}\,(1+2\alpha\mathcal{E}) \tag{51}$$

$$H_{\mathrm{M}}(\alpha\mathcal{E}) = H_{\mathrm{u}}(\alpha\mathcal{E}) H_{\mathrm{g}}(\alpha\mathcal{E}) H_{\mathcal{E}}(\alpha\mathcal{E}) = (1+\alpha\mathcal{E})^{3/2} \tag{52}$$

which will be approximated as

$$H_{\mathrm{g}}(\alpha\mathcal{E}) = 1 + \gamma_{\mathrm{g}} (\alpha\mathcal{E})^{\lambda_{\mathrm{g}}} \ , \tag{53}$$

$$H_{\mathrm{M}}(\alpha\mathcal{E}) = 1 + \gamma_{\mathrm{M}} (\alpha\mathcal{E})^{\lambda_{\mathrm{M}}} \tag{54}$$

to obtain closed form solutions. Introducing the auxiliary functions

$$M_{\mathrm{y}}(x) = \mathcal{I}_{\mathrm{y}}(x, a, b) + c_{\mathrm{A}} \, \mathcal{I}_{\mathrm{y}}(x, a_{\mathrm{c}}, 1) \tag{55}$$

and requiring that f_{A} reproduces the moments $\langle \Phi_i^{\mathbf{u}} \rangle$ we obtain a linear equation system

$$\langle \Phi_i^{\mathbf{u}} \rangle = \sum_{j=0}^{2} C_{ij} \, \mathbf{B}_j \ , \tag{56}$$

$$C_{ij} = C_{\mathrm{M}} M_{\mathrm{M}}(i+j+1) \ , \tag{57}$$

where the C_{ij} have the property $C_{ij} = C_{kl}$ for $i + j = k + l$. Solving for $\mathbf{B}_i$ gives

$$\mathbf{B}_i = \sum_{j=0}^{2} D_{ij} \langle \Phi_j^{\mathbf{u}} \rangle \tag{58}$$

where the D_{ij} are the components of the inverse matrix $\hat{\mathrm{C}}^{-1}$ which are symmetric, $D_{ij} = D_{ji}$. The anti-symmetric part of the distribution function can now be written as

$$f_{\mathrm{A}}(\mathbf{k}) = f_{\mathcal{E}}(\mathcal{E}) \sum_{i=0}^{2} d_i(\mathcal{E}) \, \langle \Phi_i^{\mathbf{u}} \rangle \cdot \mathbf{k} \tag{59}$$

$$d_i(\mathcal{E}) = \sum_{j=0}^{2} D_{ji} \, \mathcal{E}^j \ . \tag{60}$$

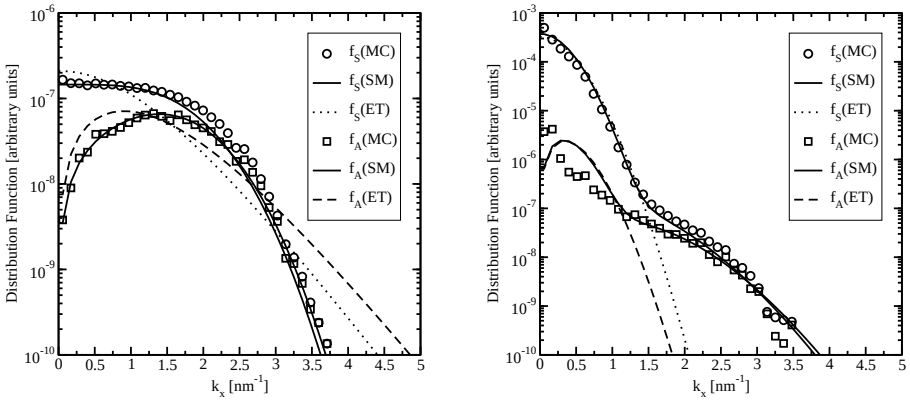

Fig. 6. Cuts through the symmetric and anti-symmetric parts of the distribution function inside the drain region (left) and at the end of the channel region (right). The symbols are the MC result while the solid lines are the analytic six moments model. Also shown is the energy-transport (ET) version.

5.3. *Energy-Transport Version*

In the following, we shortly present an energy-transport version of this model, because energy-transport models are the most commonly used extensions to drift-diffusion models. An energy-transport version of the even part is obtained by assuming $b = 1$ which gives a heated Maxwellian distribution function

$$f_{\mathrm{S}}(\mathcal{E}) = A \exp\Big[-\frac{\mathcal{E}}{a}\Big] \ . \tag{61}$$

The coefficient a is determined via the nonlinear relation

$$a = \langle \mathcal{E} \rangle \frac{1 + a^{\lambda_{\mathrm{g}}} \mathcal{A}(\frac{3}{2})}{\frac{3}{2} + a^{\lambda_{\mathrm{g}}} \mathcal{A}(\frac{5}{2})} \tag{62}$$

$$\text{with} \qquad \mathcal{A}(x) = \gamma_{\mathrm{g}} \alpha^{\lambda_{\mathrm{g}}} \frac{\Gamma(x + \lambda_{\mathrm{g}})}{\Gamma(\frac{3}{2})} \tag{63}$$

which is of course a special case of (45) and gives the expected result $\langle \mathcal{E} \rangle = 3\mathrm{k_B}T/2$ for parabolic bands. The anti-symmetric part is obtained by considering only $\mathbf{B}_0$ and $\mathbf{B}_1$ in (47) which reduces the rank of the matrices $\hat{\mathrm{C}}$ and $\hat{\mathrm{D}}$ to two.

5.4. *Evaluation of the Analytic Models*

A comparison of the analytic model with Monte Carlo data is given in Fig. 6 at the end of the channel region and at the beginning of the drain region of an n^+-n-n^+ structure with $L_{\mathrm{C}} = 100$ nm. The agreement in both regions is highly satisfactory. Also shown is the energy-transport version which is clearly not able to reproduce the basic features of the distribution function.

6. Scattering Models

By introducing a relaxation time $\tau_\phi(\mathcal{E})$ related to the weight function ϕ the scattering integral can be rearranged formally as[9]

$$\int \phi(\mathbf{k})\, Q[f(\mathbf{k})]\ \mathrm{d}^3\mathbf{k} = -n \left\langle \frac{\phi(\mathbf{k})}{\tau_\phi(\mathcal{E})} \right\rangle . \tag{64}$$

For even weight functions the relaxation time is obtained as

$$\frac{1}{\tau_\phi(\mathcal{E})} = \int \Big[1 - \frac{\phi(\mathbf{k}')}{\phi(\mathbf{k})}\Big] S(\mathbf{k},\mathbf{k}')\ \mathrm{d}^3\mathbf{k}' . \tag{65}$$

Special care has to be taken if the weight function ϕ is a vector, since division as performed in (65) is not possible. Considering $\phi = \mathbf{k}$, the momentum relaxation time $\tau_{\mathbf{p}}(\mathbf{k})$ is obtained as[29]

$$\frac{1}{\tau_p(\mathbf{k})} = \int \Big[1 - \frac{k'}{k}\cos\vartheta\Big] S(k, k'\cos\vartheta)\ \mathrm{d}^3\mathbf{k}' . \tag{66}$$

In the following we will evaluate the scattering integral considering acoustic deformation potential scattering (ADP), intravalley scattering (IVS), and impurity scattering (IMP)[29]. For IMP the Brooks-Herring model is used for simplicity, although more accurate models can be treated in the same manner. The momentum relaxation times for the three scattering processes read[29]

$$\text{ADP}: \quad \frac{1}{\tau_p(\mathcal{E})} = K_{\mathrm{adp}}\, g(\mathcal{E}) , \tag{67}$$

$$\text{IVS}: \quad \frac{1}{\tau_p^{\pm}(\mathcal{E})} = K_{\mathrm{ivs}}^{\pm}\, \sigma(\mathcal{E} \pm \mathcal{E}_0) g(\mathcal{E} \pm \mathcal{E}_0) , \tag{68}$$

$$\text{IMP}: \quad \frac{1}{\tau_p(\mathcal{E})} = K_{\mathrm{imp}}\, T(t)\, H_{\mathrm{imp}}(\alpha\mathcal{E})\, \mathcal{E}^{-3/2} , \tag{69}$$

with the auxiliary definitions for IMP

$$T(t) = \Big[\ln(1+t) - \frac{t}{1+t}\Big] \qquad \text{with} \qquad t = \frac{4}{\mathcal{E}_\beta}\mathcal{E}(1+\alpha\mathcal{E}) , \tag{70}$$

$$H_{\mathrm{imp}}(\alpha\mathcal{E}) = \frac{1+2\alpha\mathcal{E}}{(1+\alpha\mathcal{E})^{3/2}} . \tag{71}$$

The constants K_{adp}, $K_{\mathrm{ivs}}^{\pm}$, $\mathcal{E}_0$, K_{imp}, and $\mathcal{E}_\beta$ are energy-independent and standard definitions are used[9].

6.1. *Relaxation Times*

The relaxation times for the balance equations are determined by the even moments

ϕ_i which evaluate with neglected generation/recombination processes to

$$\frac{1}{\tau_{\phi_0}(\mathbf{k})} = 0 \ , \tag{72}$$

$$\frac{1}{\tau_{\phi_1}(\mathbf{k})} = \int \Big[1 - \frac{\mathcal{E}(\mathbf{k}')}{\mathcal{E}(\mathbf{k})}\Big] S(\mathbf{k},\mathbf{k}') \ \mathrm{d}^3\mathbf{k}' \ , \tag{73}$$

$$\frac{1}{\tau_{\phi_2}(\mathbf{k})} = \int \Big[1 - \frac{\mathcal{E}^2(\mathbf{k}')}{\mathcal{E}^2(\mathbf{k})}\Big] S(\mathbf{k},\mathbf{k}') \ \mathrm{d}^3\mathbf{k}' \ . \tag{74}$$

The scattering integral can then be written as

$$q_i = -\Big\langle \frac{\phi_i}{\tau_{\phi_i}(\mathcal{E})} \Big\rangle = \frac{1}{m_\mathrm{g}(0)} \int \phi_i \, \mathcal{E}^{1/2} H_\mathrm{g}(\alpha\mathcal{E}) \frac{f_\mathrm{S}(\mathcal{E})}{\tau_{\phi_i}(\mathcal{E})} \ \mathrm{d}\mathcal{E} \ . \tag{75}$$

Finally we can express the relaxation times required in the macroscopic transport equations as

$$\tau_i = \tau_{\langle\phi_i\rangle} = -\frac{\langle\phi_i\rangle - \langle\phi_i\rangle_\mathrm{eq}}{q_i} \quad \text{with} \quad \langle\phi_i\rangle_\mathrm{eq} = \frac{m_\mathrm{g}(i)}{m_\mathrm{g}(0)}\Big|_\mathrm{eq} = \frac{\mathcal{I}_\mathrm{y}(i, \mathrm{k_B}T_\mathrm{L}, 1)}{\mathcal{I}_\mathrm{y}(0, \mathrm{k_B}T_\mathrm{L}, 1)} \ . \tag{76}$$

Since ADP and IMP are assumed to be elastic, $\mathcal{E}(\mathbf{k}) = \mathcal{E}(\mathbf{k}')$, they do not contribute to these relaxation times. IVS is assumed to be isotropic with $\mathcal{E}(\mathbf{k}') = \mathcal{E} \pm \mathcal{E}_0$ which gives

$$\frac{1}{\tau_{\phi_1}(\mathcal{E})} = \mp\frac{\mathcal{E}_0}{\mathcal{E}} \int S(\mathbf{k},\mathbf{k}') \ \mathrm{d}^3\mathbf{k}' = \mp\frac{\mathcal{E}_0}{\mathcal{E}} \frac{1}{\tau_p^\pm(\mathcal{E})} \ , \tag{77}$$

$$\frac{1}{\tau_{\phi_2}(\mathcal{E})} = \Big[\mp\frac{2\mathcal{E}_0}{\mathcal{E}} - \frac{\mathcal{E}_0^2}{\mathcal{E}^2}\Big] \int S(\mathbf{k},\mathbf{k}') \ \mathrm{d}^3\mathbf{k}' = \Big[\mp\frac{2\mathcal{E}_0}{\mathcal{E}} - \frac{\mathcal{E}_0^2}{\mathcal{E}^2}\Big] \frac{1}{\tau_p^\pm(\mathcal{E})} \ . \tag{78}$$

The scattering integral is then obtained as

$$q_0 = 0 \ , \tag{79}$$

$$q_1 = \mathcal{E}_0 g_0 A \int f_\mathcal{E}(\mathcal{E}) \mathcal{E}^{1/2} H_\mathrm{g}(\alpha\mathcal{E}) \Big[\frac{1}{\tau_p^-(\mathcal{E})} - \frac{1}{\tau_p^+(\mathcal{E})}\Big] \ \mathrm{d}\mathcal{E} \ , \tag{80}$$

$$q_2 = \mathcal{E}_0 g_0 A \int f_\mathcal{E}(\mathcal{E}) \mathcal{E}^{1/2} H_\mathrm{g}(\alpha\mathcal{E}) \Big[(2\mathcal{E} - \mathcal{E}_0)\frac{1}{\tau_p^-(\mathcal{E})} - (2\mathcal{E} + \mathcal{E}_0)\frac{1}{\tau_p^+(\mathcal{E})}\Big] \ \mathrm{d}\mathcal{E} \ . \tag{81}$$

6.2. *Mobilities*

We now define the scalar mobilities μ_i which are associated with the fluxes $\Phi_i^\mathbf{u}$ via

$$-\Big\langle \frac{\Phi_i^\mathbf{P}}{\tau_p(\mathcal{E})} \Big\rangle = \mathrm{q}\frac{\langle\Phi_i^\mathbf{u}\rangle}{\mu_i} \qquad \text{with} \quad i = 0, 1, 2 \ . \tag{82}$$

Note that we *do not* employ the relaxation time approximation as we evaluate the scattering integral directly, using the microscopic relaxation times of the odd moments $\Phi_i^\mathbf{P} = \hbar\mathbf{k}\,\mathcal{E}^i$.

$$\frac{1}{\tau_{\Phi_i^\mathbf{P}}(\mathbf{k})} = \int \mathrm{d}\cos\vartheta \int k'^2 \mathrm{d}k' \Big[1 - \frac{k'}{k}\cos\vartheta \, \frac{\mathcal{E}^i(\mathbf{k}')}{\mathcal{E}^i(\mathbf{k})}\Big] S(k, k', \cos\vartheta) \tag{83}$$

Since ADP and IMP are elastic, which means $\mathcal{E}(\mathbf{k}) = \mathcal{E}(\mathbf{k}')$, but anisotropic with $S = S(k, k', \cos\vartheta)$ we obtain

$$\frac{1}{\tau_{\Phi_i^{\mathbf{P}}}(\mathbf{k})} = \int \Big[1 - \frac{k'}{k}\cos\vartheta\Big] S(\mathbf{k},\mathbf{k}')\ \mathrm{d}^3\mathbf{k}' = \frac{1}{\tau_p(\mathbf{k})} \tag{84}$$

with τ_p being the momentum relaxation time. Since IVS is isotropic with $S = S(k, k')$, the integration over ϑ yields zero and we obtain

$$\frac{1}{\tau_{\Phi_i^{\mathbf{P}}}(\mathbf{k})} = \int S(\mathbf{k},\mathbf{k}')\ \mathrm{d}^3\mathbf{k}' = \frac{1}{\tau(\mathbf{k})} = \frac{1}{\tau_p(\mathbf{k})}\ . \tag{85}$$

We can now evaluate the scattering integral using the analytic distribution function to obtain

$$-\Big\langle \frac{\Phi_i^{\mathbf{P}}}{\tau_p(\mathcal{E})} \Big\rangle = \frac{1}{n}\int \Phi_i^{\mathbf{P}}\ \frac{f_{\mathrm{A}}}{\tau_p(\mathcal{E})}\ \mathrm{d}^3\mathbf{k} \tag{86}$$

$$= C_{\mathrm{Q}} \sum_{j=0}^{2} Q_{ij}\, \mathbf{B}_j \tag{87}$$

with the definitions $C_{\mathrm{Q}} = m^*\, C_{\mathrm{M}}$ and

$$Q_{ij} = \int \mathcal{E}^{i+j+3/2} H_{\mathrm{Q}}(\alpha\mathcal{E}) \frac{f_{\mathcal{E}}(\mathcal{E})}{\tau_p(\mathcal{E})}\ \mathrm{d}\mathcal{E}\ , \tag{88}$$

$$H_{\mathrm{Q}}(\alpha\mathcal{E}) = (1+\alpha\mathcal{E})^{3/2}(1+2\alpha\mathcal{E})\ . \tag{89}$$

Substituting the already calculated coefficients $\mathbf{B}_i$ which depend on the fluxes $\langle\Phi_l^{\mathbf{u}}\rangle$ we obtain

$$-\Big\langle \frac{\Phi_i^{\mathbf{P}}}{\tau_p(\mathcal{E})} \Big\rangle = C_{\mathrm{Q}} \sum_{j=0}^{2} Q_{ij} \sum_{l=0}^{2} D_{jl} \langle\Phi_l^{\mathbf{u}}\rangle = C_{\mathrm{Q}} \sum_{j=0}^{2} \langle\Phi_j^{\mathbf{u}}\rangle \sum_{l=0}^{2} D_{lj} Q_{il} = \sum_{j=0}^{2} Z_{ij} \langle\Phi_j^{\mathbf{u}}\rangle \tag{90}$$

$$Z_{ij} = C_{\mathrm{Q}} \sum_{l=0}^{2} D_{lj} Q_{il}\ . \tag{91}$$

The scattering integral for the odd weight functions can thus be expressed as a linear combination of the fluxes with the coefficients Z_{ij} which only depend on the even moments. This is in accordance with the results obtained by Hänsch[5]. The coefficients Z_{ij} contain the information about the scattering rates via the coefficients Q_{ij} which are given as follows

$$Q_{ij}^{\mathrm{adp}} = K_{\mathrm{adp}} g_0 \int \mathcal{E}^{i+j+2} H_{\mathrm{adp}}(\alpha\mathcal{E}) f_{\mathcal{E}}(\mathcal{E})\ \mathrm{d}\mathcal{E}\ , \tag{92}$$

$$Q_{ij}^{\mathrm{ivs}} = K_{\mathrm{ivs}}^{\pm} g_0 \int \mathcal{E}^{i+j+3/2} H_{\mathrm{ivs}}^{\pm}(\mathcal{E}) f_{\mathcal{E}}(\mathcal{E})\ \mathrm{d}\mathcal{E}\ , \tag{93}$$

$$Q_{ij}^{\mathrm{imp}} = K_{\mathrm{imp}} \int \mathcal{E}^{i+j} H_{\mathrm{Q}}(\alpha\mathcal{E}) H_{\mathrm{imp}}(\gamma^2) f_{\mathcal{E}}(\mathcal{E})\ \mathrm{d}\mathcal{E}\ , \tag{94}$$

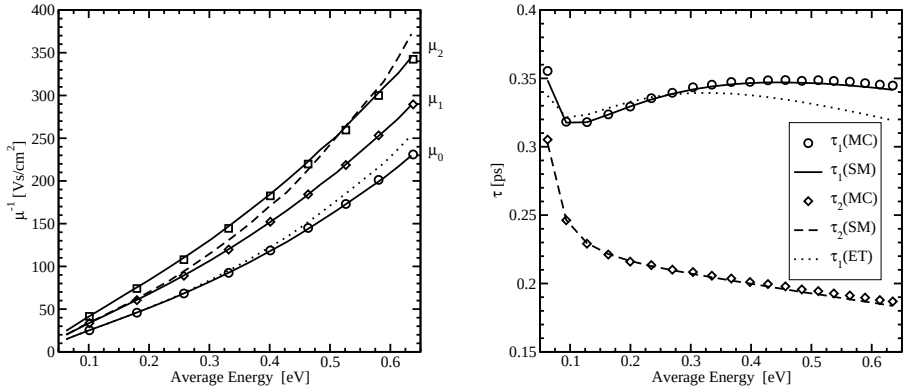

Fig. 7. Mobilities and relaxation times required for the six moments model for bulk with $E_{\max} = 200\,\mathrm{kV/cm}$. The symbols are the Monte Carlo results, whereas the lines are obtained by the analytic six moments model. The dotted line gives the result obtained by a displaced and heated Maxwellian approximation.

with the auxiliary non-parabolicity functions

$$H_{\mathrm{adp}}(\alpha\mathcal{E}) = (1+\alpha\mathcal{E})^2(1+2\alpha\mathcal{E})^2 \ , \tag{95}$$

$$H^{\pm}_{\mathrm{ivs}}(\mathcal{E}) = (1+\alpha\mathcal{E})^{3/2}(1+2\alpha\mathcal{E})\sqrt{\mathcal{E}\pm\mathcal{E}_0}H_{\mathrm{g}}(\mathcal{E}\pm\mathcal{E}_0) \ . \tag{96}$$

6.3. *Evaluation of the Scattering Models*

In our Monte Carlo code we use the same scattering rates as given above and a single equivalent isotropic non-parabolic band. Although this band structure is unreliable for energies above 0.5 eV, it allows us to write relatively simple closed form expressions when the integrals occurring in the evaluation of the scattering integral are accordingly approximated. It is believed that our approach can be extended to more accurate analytical models in a straight forward manner. We use the first six moments obtained from the Monte Carlo simulation to evaluate the distribution function model and the scattering integral. The resulting highly accurate mobilities and relaxation times are shown in Fig. 7 for a bulk simulation with $E_{\max} = 200\,\mathrm{kV/cm}$ and in Fig. 8 for an n^+-n-n^+ structure with $L_{\mathrm{C}} = 100$ nm and a maximum electric field of $E_{\max} = 100\,\mathrm{kV/cm}$. For bulk and the channel region where $c = 0$ and no heuristic criterions are applied the error in the mobilities and and relaxation times is well below 0.1%. Even in the drain region, where the bulk relation between the average of the square of the energy and the average energy is assumed to be valid, there is precise accuracy.

In Fig. 7 and Fig. 9 the analogous expressions for the energy-transport model are evaluated which clearly confirm that the resulting heated and displaced Maxwellian distribution is not well suited for the modeling of hot carrier processes. Furthermore, it might be concluded that the energy-transport model is not self-contained, in a

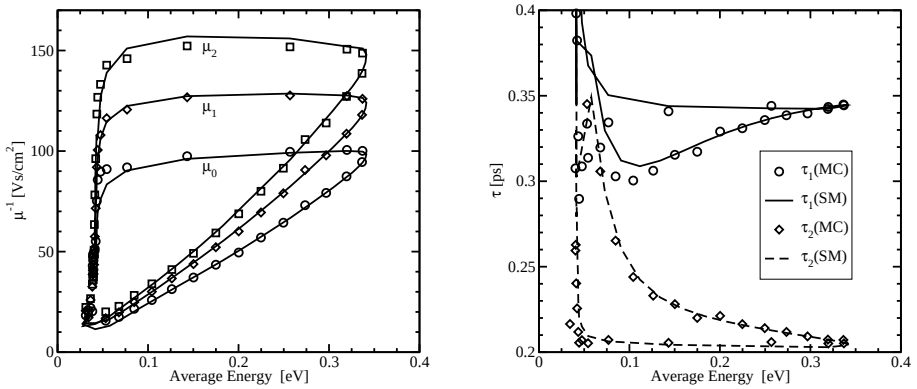

Fig. 8. Mobilities and relaxation times required for the six moments model for an n^+-n-n^+ structure with $L_\mathrm{C} = 100$ nm. The symbols are the Monte Carlo results, whereas the solid lines are obtained by the analytic six moments model.

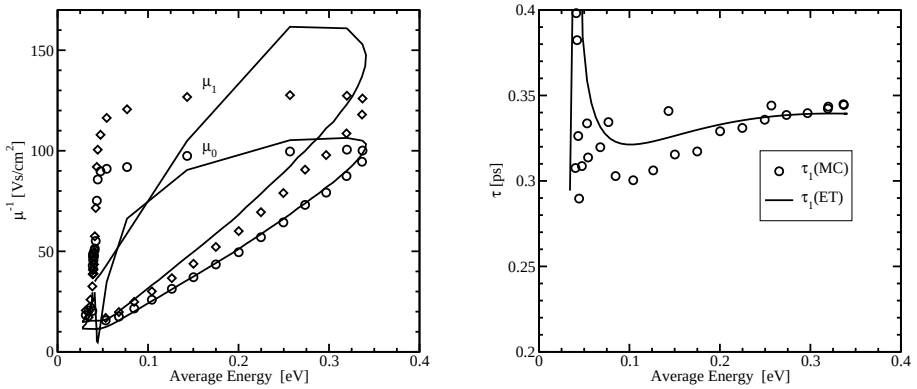

Fig. 9. Mobilities and relaxation times required for the energy-transport model predicted by the heated and displaced Maxwellian distribution function.

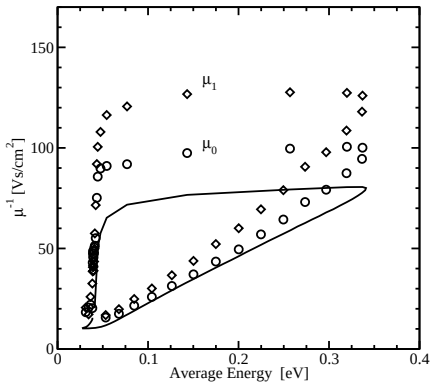

Fig. 10. The mobilities predicted by the Hänsch model. Note that $\mu_1 = \mu_0$ is frequently assumed.

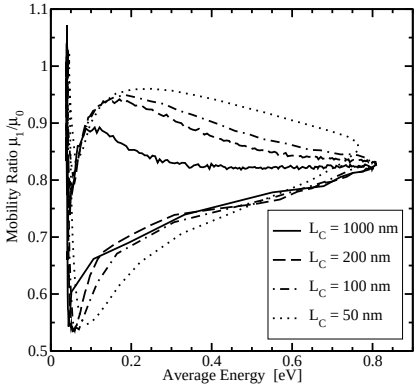

Fig. 11. Ratio of the mobilities for several n^+-n-n^+ structures. Clearly, a constant value for the ratio would be a poor approximation.

sense that it simply does not provide sufficient information to accurately model the scattering integral. The six moments model, on the other hand, can be considered self-contained because the information available about the distribution function is sufficient to accurately model the scattering integral.

In energy-transport models the carrier mobility is normally modeled using the expression proposed by Hänsch[5,30].

$$\mu_0 = \mu_{\mathrm{eq}}\Big(1 - \tfrac{3}{2}\frac{\mu_0}{\mathrm{q}\tau_1 v_s^2}\Big(\mathrm{k_B}T_{\mathrm{L}} - \tfrac{2}{5}\frac{\langle\mathbf{u}\rangle\cdot\langle\mathbf{u}\mathcal{E}\rangle}{|\langle\mathbf{u}\rangle|^2}\Big)\Big)^{-1} \tag{97}$$

Here μ_{eq} is the zero-field mobility, v_s the saturation velocity, and τ_1 the energy relaxation time which is assumed to be constant. Equation (97) is evaluated in Fig. 10 for $\tau_1 = 0.33\,\mathrm{ps}$. Furthermore, it is frequently assumed that μ_1 equals μ_0 which is definitely a rough approximation as can be seen in Fig. 11 where the ratio μ_1/μ_0 is shown for several n^+-n-n^+ structures.

7. A Six Moments Transport Model

In the following the transport equations determining the first six moments will be derived where we will restrict ourselves to parabolic bands. The macroscopic transport equations are obtained by multiplying Boltzmann's equation with the appropriate weight functions and integrating the product over $\mathbf{k}$ space. As usual, we assume that the Brillouin zone extends towards infinity which is justified because the distribution function declines exponentially[31]. We apply the weight functions ϕ_i and $\Phi_i^{\mathbf{p}}$ with $i = 0, 1, 2$ to the Boltzmann equation given by (23) and (24). We continue in the following with the unscaled version because all simplifications obtained from the diffusion limit are treated separately.

7.1. *Balance Equations*

The balance equations of the six moments transport model, which are obtained as the moments of (23) with the weight function ϕ_i, take the following general form

$$\partial_t n\,\langle\phi_i\rangle + \nabla_{\mathbf{r}}\cdot n\,\langle\mathbf{u}\,\phi_i\rangle - n\,\mathbf{F}\cdot\langle\nabla_{\mathbf{p}}\,\phi_i\rangle = \int \phi_i\, Q_{\mathrm{S}}[f_{\mathrm{S}}]\;\mathrm{d}^3\mathbf{k}\;. \tag{98}$$

The calculation of the gradients of the even weight functions ϕ_i is straightforward and gives

$$\nabla_{\mathbf{p}}\,\phi_0 = 0\;, \qquad \nabla_{\mathbf{p}}\,\phi_1 = \mathbf{u}\;, \qquad \text{and} \qquad \nabla_{\mathbf{p}}\,\phi_2 = 2\,\mathcal{E}\,\mathbf{u}\;. \tag{99}$$

The balance equations can thus be written as

$$\partial_t n \qquad + \nabla_{\mathbf{r}}\cdot n\,\langle\mathbf{u}\rangle \qquad\qquad\qquad\qquad = 0\;, \tag{100}$$

$$\partial_t n\,\langle\mathcal{E}\rangle \;+ \nabla_{\mathbf{r}}\cdot n\,\langle\mathbf{u}\mathcal{E}\rangle \;-\; n\,\mathbf{F}\cdot\langle\mathbf{u}\rangle \;= -n\,\frac{\langle\mathcal{E}\rangle - \langle\mathcal{E}\rangle_{\mathrm{eq}}}{\tau_1}\;, \tag{101}$$

$$\partial_t n\,\langle\mathcal{E}^2\rangle + \nabla_{\mathbf{r}}\cdot n\,\langle\mathbf{u}\mathcal{E}^2\rangle \;-\; 2\,n\,\mathbf{F}\cdot\langle\mathbf{u}\mathcal{E}\rangle = -n\,\frac{\langle\mathcal{E}^2\rangle - \langle\mathcal{E}^2\rangle_{\mathrm{eq}}}{\tau_2}\;, \tag{102}$$

where the definitions of the relaxation times τ_i (76) have been used.

7.2. *Flux Equations*

For the formulation of the flux equations we apply the weight functions

$$\Phi_i^{\mathbf{p}} = \mathbf{p}\mathcal{E}^i = \hbar\mathbf{k}\mathcal{E}^i \tag{103}$$

to (24) and obtain

$$\nabla_{\mathbf{r}} \cdot n \langle \mathbf{u} \otimes \Phi_i^{\mathbf{p}} \rangle - n\,\mathbf{F} \cdot \langle \nabla_{\mathbf{p}} \otimes \Phi_i^{\mathbf{p}} \rangle = \int \Phi_i^{\mathbf{p}}\, Q_{\mathrm{A}}[f_{\mathrm{A}}]\, \mathrm{d}^3\mathbf{k} \ . \tag{104}$$

Equations (98) and (104) contain several gradients of scalar and vectorial functions which will be evaluated in the following. Note that the two identities which represent the gradients of a scalar- and a vector-field are helpful

$$\nabla_{\mathbf{p}}\, p = \mathbf{e}_p = \frac{\mathbf{p}}{p} \qquad \text{and} \qquad \nabla_{\mathbf{p}} \otimes \mathbf{p} = \hat{\mathrm{I}} \tag{105}$$

where $\hat{\mathrm{I}}$ is the unity tensor and $p = |\mathbf{p}|$.

For $i \geq 1$ the gradients of the odd weight functions $\Phi_i^{\mathbf{p}}$ can be written as

$$\nabla_{\mathbf{p}} \otimes \Phi_i^{\mathbf{p}} = \nabla_{\mathbf{p}} \otimes \mathbf{p}\,\mathcal{E}^i = \mathcal{E}^i\, \nabla_{\mathbf{p}} \otimes \mathbf{p} + \mathbf{p} \otimes \nabla_{\mathbf{p}} \mathcal{E}^i = \mathcal{E}^i\, \hat{\mathrm{I}} + (\mathbf{u} \otimes \mathbf{p})\, i\, \mathcal{E}^{i-1} \ . \tag{106}$$

The tensor product $\nabla_{\mathbf{p}} \otimes \Phi_i^{\mathbf{p}}$ thus evaluates to

$$i = 0: \qquad \nabla_{\mathbf{p}} \otimes \mathbf{p} \qquad = \hat{\mathrm{I}}\,, \tag{107}$$

$$i = 1: \qquad \nabla_{\mathbf{p}} \otimes (\mathbf{p}\,\mathcal{E}) \ = \hat{\mathrm{I}}\,\mathcal{E} \ + \quad \mathbf{u} \otimes \mathbf{p}\,, \tag{108}$$

$$i = 2: \qquad \nabla_{\mathbf{p}} \otimes (\mathbf{p}\,\mathcal{E}^2) = \hat{\mathrm{I}}\,\mathcal{E}^2 + 2\,\mathbf{u} \otimes \mathbf{p}\,\mathcal{E}\ . \tag{109}$$

Here we have introduced the energy tensors $\hat{\mathrm{U}}_i$ which are defined as

$$\hat{\mathrm{U}}_i = \langle \mathbf{u} \otimes \mathbf{p}\,\mathcal{E}^{i-1} \rangle = \frac{\hbar^2}{m^*} \langle \mathbf{k} \otimes \mathbf{k}\,\mathcal{E}^{i-1} \rangle \tag{110}$$

for parabolic bands. For the evaluation of (110) we note that the integral

$$n \langle \mathbf{k} \otimes \mathbf{k}\,\mathcal{E}^{i-1} \rangle = \int \mathbf{k} \otimes \mathbf{k}\,\mathcal{E}^{i-1}\, f_{\mathrm{S}}(\mathbf{k})\, \mathrm{d}^3\mathbf{k} \tag{111}$$

depends only on the symmetric part of the distribution function $f_{\mathrm{S}}(\mathbf{k})$. Under the assumption that $f_{\mathrm{S}}(\mathbf{k})$ is isotropic, that is, $f_{\mathrm{S}}(\mathbf{k}) = f_{\mathrm{S}}(|\mathbf{k}|)$, all non-diagonal elements vanish for symmetry reasons.

Since the distribution function is assumed to be isotropic, the integrals determining the diagonal elements all evaluate to a common value K

$$\langle k_l\, k_l \rangle = \frac{1}{n} \iiint_{-\infty}^{\infty} k_l^2 f_{\mathrm{S}} \left(\sqrt{k_x^2 + k_y^2 + k_z^2} \right) \mathrm{d}k_x\, \mathrm{d}k_y\, \mathrm{d}k_z = K \ , \qquad l = x, y, z \ , \tag{112}$$

which evaluates to $K = \langle k^2 \rangle / 3$. Therefore, the statistical averages of the tensors are diagonal with all diagonal elements being equal:

$$\hat{\mathrm{U}}_i \approx \frac{\hbar^2}{3m^*} \langle \mathcal{E}^{i-1}\, k^2 \rangle\, \hat{\mathrm{I}} = \tfrac{2}{3} \langle \mathcal{E}^i \rangle\, \hat{\mathrm{I}} = U_i\, \hat{\mathrm{I}} \; . \tag{113}$$

Using (113) allows one to write the average $\langle \nabla_{\mathbf{p}} \otimes \Phi_i^{\mathbf{P}} \rangle$ as

$$i = 0: \qquad \langle \nabla_{\mathbf{p}} \otimes \mathbf{p} \rangle \qquad = \hat{\mathrm{I}} \tag{114}$$

$$i = 1: \qquad \langle \nabla_{\mathbf{p}} \otimes (\mathbf{p}\, \mathcal{E}) \rangle \;= \hat{\mathrm{I}}\, \langle \mathcal{E} \rangle + \langle \mathbf{u} \otimes \mathbf{p} \rangle \qquad = \hat{\mathrm{I}}\, \langle \mathcal{E} \rangle + \hat{\mathrm{U}}_1 \quad = \hat{\mathrm{I}}\, \tfrac{5}{3}\, \langle \mathcal{E} \rangle \tag{115}$$

$$i = 2: \qquad \langle \nabla_{\mathbf{p}} \otimes (\mathbf{p}\, \mathcal{E}^2) \rangle = \hat{\mathrm{I}}\, \langle \mathcal{E}^2 \rangle + 2 \langle \mathbf{u} \otimes \mathbf{p}\, \mathcal{E} \rangle = \hat{\mathrm{I}}\, \langle \mathcal{E}^2 \rangle + 2 \hat{\mathrm{U}}_2 = \hat{\mathrm{I}}\, \tfrac{7}{3}\, \langle \mathcal{E}^2 \rangle \tag{116}$$

The flux relations then take the following form:

$$\tfrac{2}{3}\, \nabla n \langle \mathcal{E} \rangle \; - \quad n\, \mathbf{F}\, \langle 1 \rangle \;\; = -\mathrm{q}\, n\, \frac{\langle \mathbf{u} \rangle}{\mu_0} \; , \tag{117}$$

$$\tfrac{2}{3}\, \nabla n \langle \mathcal{E}^2 \rangle - \tfrac{5}{3}\, n\, \mathbf{F}\, \langle \mathcal{E} \rangle \;\; = -\mathrm{q}\, n\, \frac{\langle \mathbf{u}\mathcal{E} \rangle}{\mu_1} \; , \tag{118}$$

$$\tfrac{2}{3}\, \nabla n \langle \mathcal{E}^3 \rangle - \tfrac{7}{3}\, n\, \mathbf{F}\, \langle \mathcal{E}^2 \rangle = -\mathrm{q}\, n\, \frac{\langle \mathbf{u}\mathcal{E}^2 \rangle}{\mu_2} \; . \tag{119}$$

7.3. *Conventional Variables*

We now rewrite the above equations using the conventional variables[14]

$$\langle \mathbf{u} \rangle \;\; = \mathbf{V} \; , \qquad \langle \mathbf{u}\mathcal{E} \rangle = \mathbf{S} \; , \qquad \langle \mathbf{u}\mathcal{E}^2 \rangle = \mathbf{K} \; , \tag{120}$$

$$\langle 1 \rangle \;\; = 1 \; , \qquad \langle \mathcal{E} \rangle \;\; = \tfrac{3}{2}\, \mathrm{k_B}\, T_n \; , \qquad \langle \mathcal{E}^2 \rangle \;\; = \tfrac{5 \cdot 3}{4}\, \mathrm{k_B^2}\, T_n^2\, \beta_n \; , \tag{121}$$

$$\langle \mathcal{E}^3 \rangle = \tfrac{7 \cdot 5 \cdot 3}{8}\, \mathrm{k_B^3}\, M_6 \; . \tag{122}$$

Here, $\mathbf{V}$ is the average velocity, $\mathbf{S}$ the average energy flux, $\mathbf{K}$ the average kurtosis flux, T_n the average temperature, and β_n the kurtosis. M_6 represents the highest order moment which would be determined by the next higher equation. As the equation hierarchy is truncated here, we have to express M_6 using the available lower order moments. For a Maxwellian distribution function and parabolic bands we find that $M_6 = T_n^3$. As we have the kurtosis of the distribution function β_n available, we suggested the following empirical closure relations[14]

$$M_6 = T_n^3\, \beta_n^c \qquad \text{with} \quad c = 0,\, 1,\, 2, \text{ and } 3 \; . \tag{123}$$

The ratio M_6^{MC} / M_6 is shown in Fig. 12 for two n^+-n-n^+ structures with $L_{\mathrm{C}} = 1000$ nm and $L_{\mathrm{C}} = 100$ nm, respectively. As can be seen, $c = 3$ gives the smallest deviation from the desired value, one. In addition $c = 3$ proved to be numerically more stable than other versions. Especially for $c = 0$, which corresponds to closing the system with a Maxwellian[13] the Newton procedure fails to converge in most cases.

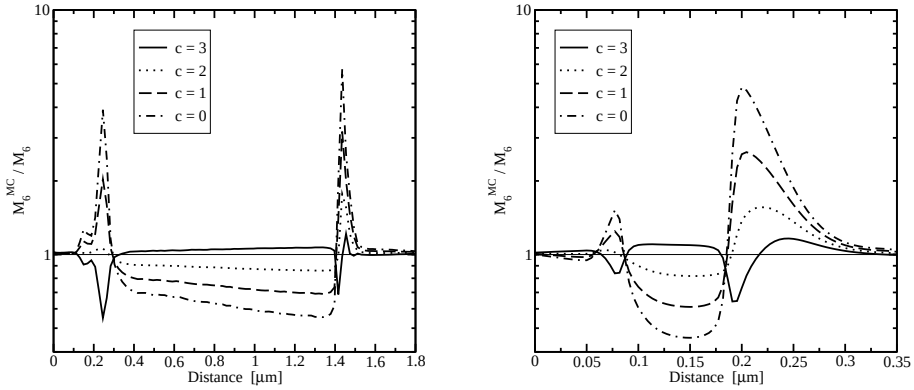

Fig. 12. Comparison of the different closure relations for a n^+-n-n^+ structure with $L_\mathrm{C} = 1000$ nm (left) and $L_\mathrm{C} = 100$ nm (right).

The final parabolic six moments model thus consists of the three flux relations

$$n\mathbf{V} = -C_0 \left(\nabla(n\,T_n) \quad + \frac{\mathrm{q}}{\mathrm{k_B}}\,\mathbf{E}\,n \right) , \qquad C_0 = \frac{\mathrm{k_B}}{\mathrm{q}}\mu_0 , \tag{124}$$

$$n\mathbf{S} \ = -C_1 \left(\nabla(n\,T_n^2\,\beta_n) + \frac{\mathrm{q}}{\mathrm{k_B}}\,\mathbf{E}\,n\,T_n \right) , \qquad C_1 = \frac{5}{2}\,\frac{\mathrm{k_B^2}}{\mathrm{q}}\,\mu_1 , \tag{125}$$

$$n\mathbf{K} = -C_2 \left(\nabla(n\,T_n^3\,\beta_n^c) + \frac{\mathrm{q}}{\mathrm{k_B}}\,\mathbf{E}\,n\,T_n^2\,\beta_n \right) , \qquad C_2 = \frac{35}{4}\,\frac{\mathrm{k_B^3}}{\mathrm{q}}\,\mu_2 , \tag{126}$$

together with the three balance equations

$$\nabla \cdot n\mathbf{V} = -\partial_t n , \tag{127}$$

$$\nabla \cdot n\mathbf{S} \ = -\tfrac{3}{2}\mathrm{k_B}\,\partial_t(n\,T_n) \qquad - \mathrm{q}\,n\,\mathbf{E}\cdot\mathbf{V} \ - \tfrac{3}{2}\mathrm{k_B}\,n\,\frac{T_n - T_\mathrm{L}}{\tau_1} , \tag{128}$$

$$\nabla \cdot n\mathbf{K} = -\tfrac{15}{4}\,\mathrm{k_B^2}\,\partial_t(n\,T_n^2\,\beta_n) - 2\,\mathrm{q}\,n\,\mathbf{E}\cdot\mathbf{S} - \tfrac{15}{4}\,\mathrm{k_B^2}\,n\,\frac{T_n^2\,\beta_n - T_\mathrm{L}^2}{\tau_2} . \tag{129}$$

7.4. *Influence of the Anisotropy of the Distribution Function*

In the derivation the symmetric part of the distribution function has been assumed isotropic. It is commonly justified by the fact that scattering is strong. A cut through the k_x, k_y-plane of the symmetric and anti-symmetric part of the distribution function at the end of the channel region of an n^+-n-n^+ structure with $L_\mathrm{C} = 100$ nm is shown in Fig. 13 and Fig. 14, respectively. The solid lines represent rigorous MC results, whereas the dashed lines are from calculations with an isotropic analytical model. A slight anisotropy is visible as the real distribution function is narrower in the direction perpendicular to the current flow.

One consequence of the assumped isotropy is that within the diffusion approxima-

tion the energy tensors

$$\hat{\mathrm{U}}_i = \langle \mathbf{u} \otimes \mathbf{p}\, \mathcal{E}^{i-1} \rangle = U_i\, \hat{\mathrm{I}} \tag{130}$$

are diagonal tensors where all diagonal elements have the same value U_i. For example, with $i = 1$ we obtain as a consequence a scalar carrier temperature T_n. In general, however, the elements of the energy tensors are not equal. Particularly the element in the direction of the current flow may contain a significant kinetic component which is neglected in the diffusion approximation because of (35) and (36). The kinetic component can be identified in a general way by separating the group velocity $\mathbf{u}$ into a random part $\mathbf{u}_c$ and the mean value $\mathbf{V} = \langle \mathbf{u} \rangle$ as $\mathbf{u} = \mathbf{u}_c + \mathbf{V}$ and the carrier momentum $\mathbf{p}$ into $\mathbf{p}_c$ and its mean value $\mathbf{P} = \langle \mathbf{p} \rangle$ as $\mathbf{p} = \mathbf{p}_c + \mathbf{P}$. The energy tensors can then be written as

$$\hat{\mathrm{U}}_i = \langle \mathbf{u} \otimes \mathbf{p}\, \mathcal{E}^{i-1} \rangle = \langle \mathbf{u}_c \otimes \mathbf{p}_c\, \mathcal{E}^{i-1} \rangle + \mathbf{V} \otimes \mathbf{P}\, \langle \mathcal{E}^{i-1} \rangle \tag{131}$$

Using the same value U_i for all tensor components implies that the influence of thermal diffusion on the current is overestimated in the direction normal to the current flow. A striking manifestation of the consequences can be observed in the simulation of MOS transistors where the electron concentration obtained by energy-transport models spreads much deeper into the bulk than would be expected from MC simulations. A typical situation is depicted in Fig. 15 where the electron concentration of a MOS transistor with $L_\mathrm{g} = 130\,\mathrm{nm}$ resulting from a MC simulation is compared to that of an energy-transport simulation. The overestimated spreading of the carriers in the energy-transport simulation can be clearly seen.

In a recent study[26] this effect has been related to errors introduced by assuming an isotropic distribution function and by the closure of the energy-transport equation system where a heated Maxwellian is assumed. The ratio of the temperature tensor components are shown in Fig. 16 for two n^+-n-n^+ structures and three MOS transistors. As the energy is assumed to be equally partitioned over the components of the temperature tensor, an overestimation of the temperature component into the bulk is obtained. Note that fairly artificial measures like reducing the heat flux by a small factor[32,33] should be used with care.

This enhanced spreading of the carriers into the bulk leads to a complete breakdown of the energy-transport model in the case of partially depleted SOI transistors where the excess carriers recombine in the bulk and virtually turn the transistor off via the bulk effect. A modified energy-transport model has been proposed[26] where both the closure and the anisotropy is modeled based on empirical corrections. In MOS transistors this effect is much less important and has as such been considered only as a cosmetic problem of energy-transport models as the body potential is not influenced by this effect.

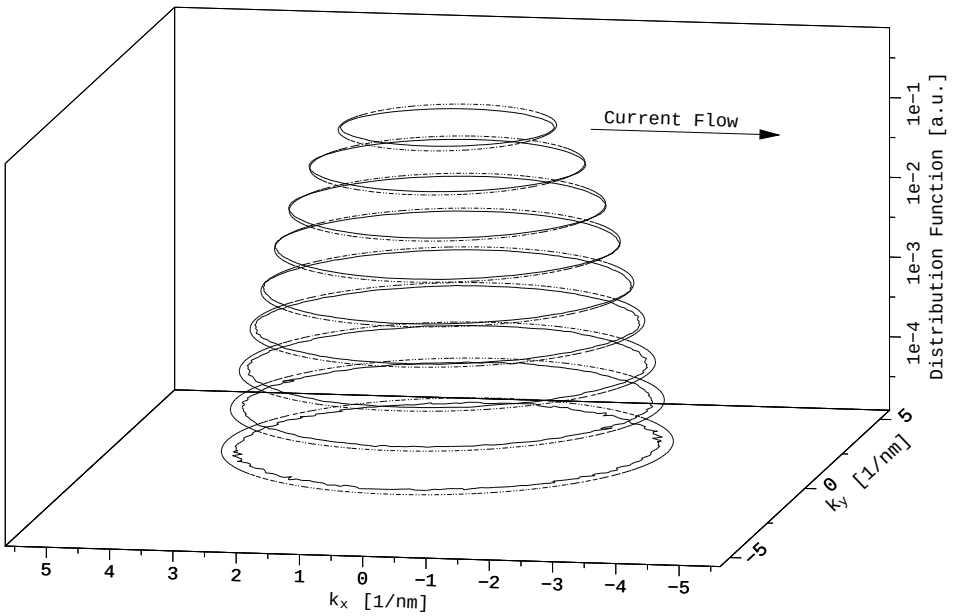

Fig. 13. Cut through the k_x, k_y-plane of the symmetric part of the distribution function at the end of the channel region of an n^+-n-n^+ structure with $L_\mathrm{C} = 100$ nm. The solid lines give the MC results, whereas the dashed lines are from the analytical model.

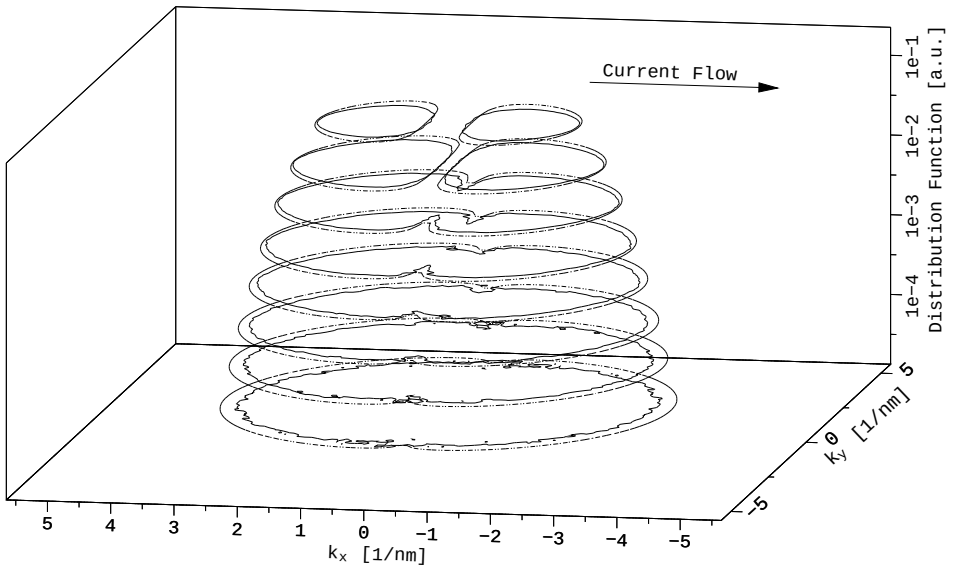

Fig. 14. Cut through the k_x, k_y-plane of the absolute value of the anti-symmetric part of the distribution function at the end of the channel region of an n^+-n-n^+ structure with $L_\mathrm{C} = 100$ nm. The solid lines give the MC results, whereas the dashed lines are from the analytical model.

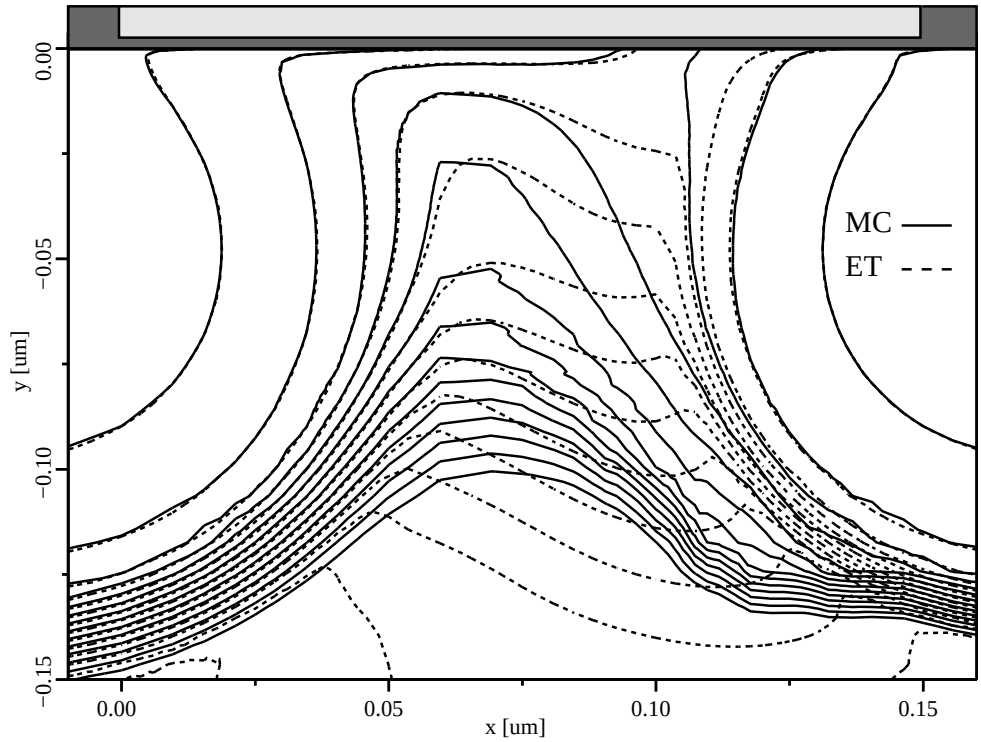

Fig. 15. Comparison of the simulated electron concentration of a MOS transistor with $L_{\mathrm{g}} = 130\,\mathrm{nm}$ from a MC simulation and an energy-transport (ET) model. Neighboring lines differ by a factor of 10. The overestimated carrier spreading into the bulk in the ET simulation can be clearly seen.

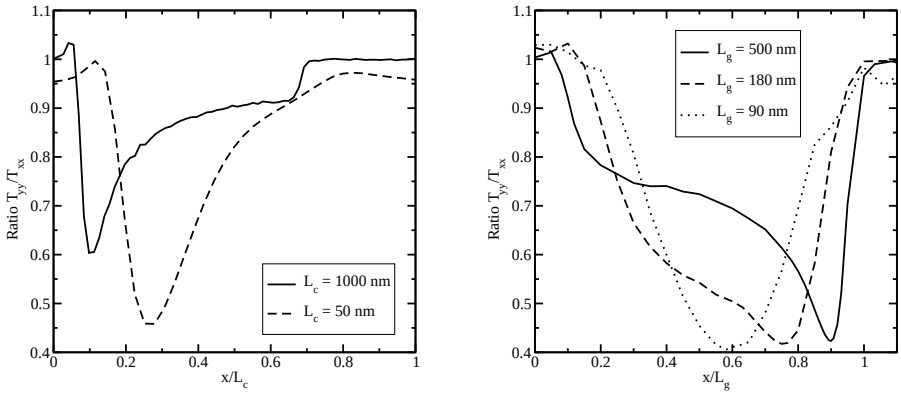

Fig. 16. Ratio of the temperature tensor components T_{yy} and T_{xx} in small n^+-n-n^+ structures (left) and small MOS transistors (right).

8. Application

With the analytical distribution function model at hand it is in principle straight forward to transfer microscopic scattering rates in models suitable for macroscopic transport models. So far, the heated Maxwellian approximation has been used for this purpose, giving unsatisfactory results. In the previous sections we have already demonstrated how the scattering integral can be directly evaluated using the analytic distribution function model with superior results as compared to the heated Maxwellian approximation. The same procedure can be applied to other scattering processes, in particular hot carrier processes which depend even stronger on the shape of the distribution function. Since impact ionization is a very important hot carrier effect, causing substrate currents and gate oxide degradation, it will be considered in the following, as notoriously poor results are obtained within energy-transport models.

8.1. *Impact Ionization*

A closed form macroscopic impact ionization rate is obtained by integrating Keldysh's expression[34] against the analytic distribution function (37).

$$P_{\mathrm{II}}(\mathcal{E}) = P_0 \Big(\frac{\mathcal{E} - \mathcal{E}_{\mathrm{th}}}{\mathcal{E}_{\mathrm{th}}} \Big)^2 \,. \tag{132}$$

Using (14) and (37) we obtain[11,35]

$$G_{\mathrm{II},i} = \int_{\mathcal{E}_{\mathrm{th}}}^{\infty} \mathcal{E}^i \, P_{\mathrm{II}}(\mathcal{E}) \, f(\mathcal{E}) \, g(\mathcal{E}) \, \mathrm{d}\mathcal{E} \tag{133}$$

$$\approx \int_{\mathcal{E}_{\mathrm{th}}}^{\infty} \mathcal{E}^i \, P_{\mathrm{II}}(\mathcal{E}) \, f_{\mathrm{h}}(\mathcal{E}) \, g_{\mathrm{c}}(\mathcal{E}) \, \mathrm{d}\mathcal{E} \tag{134}$$

$$= P_0 \, \frac{n}{m_{\mathrm{g}}(0)} \, \frac{a^{i+\frac{3}{2}}}{b} \Big(\frac{a}{\mathcal{E}_{\mathrm{C}}} \Big)^{\lambda_{\mathrm{c}} - \frac{1}{2}} \Big(\Gamma_{i,1} - 2 {z_{\mathrm{th}}}^{-\frac{1}{b}} \, \Gamma_{i,2} + {z_{\mathrm{th}}}^{-\frac{2}{b}} \, \Gamma_{i,3} \Big) \,, \tag{135}$$

where $\Gamma(a, z)$ is the incomplete Gamma function and

$$\Gamma_{i,j} = \Gamma\Big(\frac{i + j + \lambda_{\mathrm{c}}}{b}, z_{\mathrm{th}} \Big) \,, \tag{136}$$

$$z_{\mathrm{th}} = \Big(\frac{\mathcal{E}_{\mathrm{th}}}{a} \Big)^b \,, \tag{137}$$

$$g_{\mathrm{c}}(\mathcal{E}) = g_0 \sqrt{\mathcal{E}_{\mathrm{C}}} \Big(\frac{\mathcal{E}}{\mathcal{E}_{\mathrm{C}}} \Big)^{\lambda_{\mathrm{c}}} \,. \tag{138}$$

Equation (138) is an approximation of the high-energy region of the density of states ($\mathcal{E}_{\mathrm{C}} = 0.35\,\mathrm{eV}$ and $\lambda = 1.326$) based on Cassi and Riccò's[24] model, which has been introduced to simplify the final expression. Furthermore, it is assumed that only $f_{\mathrm{h}}(\mathcal{E})$ contributes to the impact ionization rate. In (135) $i = 0, 1, 2$ and denotes the entries for the continuity, energy balance, and kurtosis balance equations, respectively.

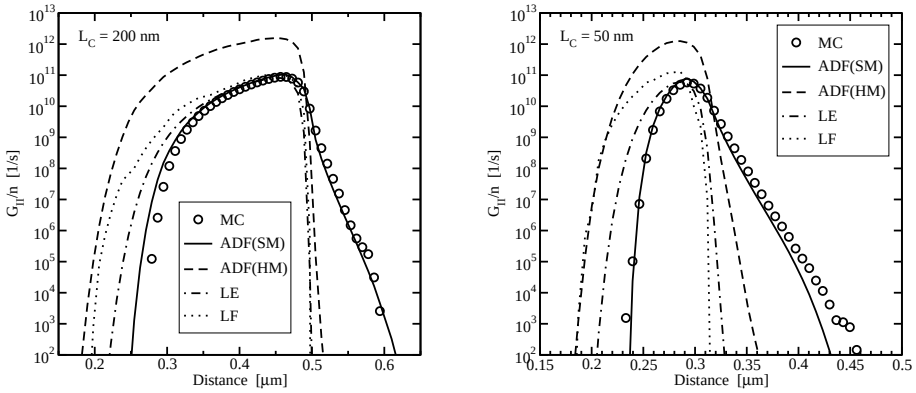

Fig. 17. Analytical impact ionization rates in comparison with Monte Carlo data for two n^+-n-n^+ structures. The ADF models use analytical models for the distribution function, either based on six moments (SM) or a heated Maxwellian distribution (HM). Also shown are the empirical models based on the local field (LF) and the local energy (LE).

A comparison with Monte Carlo data is shown in Fig. 17 where the analytical models have been evaluated using the moments obtained by Monte Carlo simulations. The model based on (37) delivers highly accurate results for both devices. It is important to note that when a heated Maxwellian is assumed instead of (37), the results deteriorate. This is frequently performed in physics based models[7]. Also shown are the results obtained by two commonly used empirical fit models[8]

$$G_{\mathrm{II}}^{\mathrm{LF}} = n\, g_{\mathrm{II}}\, \exp\Big(-\frac{E_C}{|\mathbf{E}|}\Big)\ , \tag{139}$$

$$G_{\mathrm{II}}^{\mathrm{LE}} = n\, g_{\mathrm{II}}\, \exp\Big(-\frac{\mathcal{E}_C}{\mathrm{k_B}\, T_n}\Big)\ . \tag{140}$$

These models use the local field (LF) and on the local energy (LE) as parameters. To match the Monte Carlo results the LF and LE models have been calibrated, whereas the same impact ionization parameters as in the Monte Carlo simulation were used for the models based on the analytical distribution function.

9. Conclusions

We present a six moments transport model which also the kurtosis of the distribution function as a solution variable. The kurtosis gives a significant improvement in the accuracy of distribution function models. This accuracy is exploited for modeling mobilities and relaxation times by evaluating the scattering integral where highly satisfactory results have been achieved. From these results it might be concluded that the energy-transport model is not self-contained, in a sense that it simply does not provide sufficient information to accurately model the scattering integral, whereas the six moments model is Thus, we consider the six moments transport model a balanced trade-off between accuracy and complexity.

10. References

1. S. Selberherr, *Analysis and Simulation of Semiconductor Devices*. Wien–New York: Springer, 1984.
2. R. Stratton, "Diffusion of Hot and Cold Electrons in Semiconductor Barriers," *Physical Review*, vol. 126, no. 6, pp. 2002–2014, 1962.
3. K. Bløtekjær, "Transport Equations for Electrons in Two-Valley Semiconductors," *IEEE Trans.Electron Devices*, vol. 17, no. 1, pp. 38–47, 1970.
4. T. Grasser, T. Tang, H. Kosina, and S. Selberherr, "A Review of Hydrodynamic and Energy-Transport Models for Semiconductor Device Simulation," *Proc.IEEE*, vol. 91, no. 2, pp. 251–274, 2003.
5. W. Hänsch, *The Drift Diffusion Equation and its Application in MOSFET Modeling*. Wien–New York: Springer, 1991.
6. G. Baccarani and M. Wordeman, "An Investigation of Steady-State Velocity Overshoot in Silicon," *Solid-State Electron.*, vol. 28, no. 4, pp. 407–416, 1985.
7. W. Quade, E. Schöll, and M. Rudan, "Impact Ionization within the Hydrodynamic Approach to Semiconductor Transport," *Solid-State Electron.*, vol. 36, no. 10, pp. 1493–1505, 1993.
8. K. Souissi, F. Odeh, H. Tang, A. Gnudi, and P. Lu, "Investigation of the Impact Ionization in the Hydrodynamic Model," *IEEE Trans.Electron Devices*, vol. 40, no. 8, pp. 1501–1507, 1993.
9. M. Lundstrom, *Fundamentals of Carrier Transport*. Cambridge University Press, 2000.
10. A. Abramo and C. Fiegna, "Electron Energy Distributions in Silicon at Low Applied Voltages and High Electric Fields," *J.Appl.Phys.*, vol. 80, no. 2, pp. 889–893, 1996.
11. T. Grasser, H. Kosina, and S. Selberherr, "Influence of the Distribution Function Shape and the Band Structure on Impact Ionization Modeling," *J.Appl.Phys.*, vol. 90, no. 12, pp. 6165–6171, 2001.
12. A. Gehring, T. Grasser, H. Kosina, and S. Selberherr, "Simulation of Hot-Electron Oxide Tunneling Current Based on a Non-Maxwellian Electron Energy Distribution Function," *J.Appl.Phys.*, vol. 92, no. 10, pp. 6019–6027, 2002.
13. K. Sonoda, M. Yamaji, K. Taniguchi, C. Hamaguchi, and S. Dunham, "Moment Expansion Approach to Calculate Impact Ionization Rate in Submicron Silicon Devices," *J.Appl.Phys.*, vol. 80, no. 9, pp. 5444–5448, 1996.
14. T. Grasser, H. Kosina, M. Gritsch, and S. Selberherr, "Using Six Moments of Boltzmann's Transport Equation for Device Simulation," *J.Appl.Phys.*, vol. 90, no. 5, pp. 2389–2396, 2001.
15. T. Grasser, H. Kosina, C. Heitzinger, and S. Selberherr, "Characterization of the Hot Electron Distribution Function Using Six Moments," *J.Appl.Phys.*, vol. 91, no. 6, pp. 3869–3879, 2002.
16. D. Ferry, *Semiconductors*. New York: Macmillan, 1991.
17. E. Azoff, "Generalized Energy-Momentum Conservation Equation in the Relaxation Time Approximation," *Solid-State Electron.*, vol. 30, no. 9, pp. 913–917, 1987.
18. C. Gardner, "The Classical and Quantum Hydrodynamic Models," in *Proc. Intl. Workshop on Computational Electronics*, (University of Leeds), pp. 25–36, Aug. 1993.
19. M. Vecchi and M. Rudan, "Modeling Electron and Hole Transport with Full-Band Structure Effects by Means of the Spherical-Harmonics Expansion of the BTE," *IEEE Trans.Electron Devices*, vol. 45, no. 1, pp. 230–238, 1998.
20. C.-K. Lin, N. Goldsman, I. Mayergoyz, S. Aronowitz, and N. Belova, "Advances in

Spherical Harmonic Device Modeling: Calibration and Nanoscale Electron Dynamics," in *Proc. Simulation of Semiconductor Processes and Devices*, (Kyoto, Japan), pp. 167–170, Sept. 1999.
21. S.-C. Lee and T. Tang, "Transport Coefficients for a Silicon Hydrodynamic Model Extracted from Inhomogeneous Monte-Carlo Calculations," *Solid-State Electron.*, vol. 35, no. 4, pp. 561–569, 1992.
22. G. Wolokin and J. Frey, "Overshoot Effects in the Relaxation Time Approximation," in *Proc.NASECODE VIII*, (Vienna), pp. 107–108, 1992.
23. E. Kane, "Band Structure of Indium Antimonide," *J.Phys.Chem.Solids*, vol. 1, pp. 249–261, 1957.
24. D. Cassi and B. Riccò, "An Analytical Model of the Energy Distribution of Hot Electrons," *IEEE Trans.Electron Devices*, vol. 37, no. 6, pp. 1514–1521, 1990.
25. C. Ringhofer, C. Schmeiser, and A. Zwirchmayer, "Moment Methods for the Semiconductor Boltzmann Equation in Bounded Position Domains," *SIAM J.Numer.Anal.*, vol. 39, no. 3, pp. 1078–1095, 2001.
26. M. Gritsch, H. Kosina, T. Grasser, and S. Selberherr, "Revision of the Standard Hydrodynamic Transport Model for SOI Simulation," *IEEE Trans.Electron Devices*, vol. 49, no. 10, pp. 1814–1820, 2002.
27. C. Gardner, J. Jerome, and D. Rose, "Numerical Methods for the Hydrodynamic Device Model: Subsonic Flow," *IEEE Trans.Computer-Aided Design*, vol. 8, no. 5, pp. 501–507, 1989.
28. C. Gardner, "Numerical Simulation of a Steady-State Electron Shock Wave in a Submicrometer Semiconductor Device," *IEEE Trans.Electron Devices*, vol. 38, no. 2, pp. 392–398, 1991.
29. C. Jacoboni and P. Lugli, *The Monte Carlo Method for Semiconductor Device Simulation*. Wien-New York: Springer, 1989.
30. W. Hänsch and M. Miura-Mattausch, "The Hot-Electron Problem in Small Semiconductor Devices," *J.Appl.Phys.*, vol. 60, no. 2, pp. 650–656, 1986.
31. D. Woolard, H. Tian, R. Trew, M. Littlejohn, and K. Kim, "Hydrodynamic Electron-Transport Model: Nonparabolic Corrections to the Streaming Terms," *Physical Review B*, vol. 44, no. 20, pp. 11119–11132, 1991.
32. I. Bork, C. Jungemann, B. Meinerzhagen, and W. Engl, "Influence of Heat Flux on the Accuracy of Hydrodynamic Models for Ultra-Short Si MOSFETs," in *Intl. Workshop on Numerical Modeling of Processes and Devices for Integrated Circuits NUPAD V*, (Honolulu), pp. 63–66, 1994.
33. B. Fischer, *A Full-Band Monte Carlo Charge Transport Model for Nanoscale Silicon Devices Including Strain*. Shaker Verlag, 2000.
34. L. Keldysh, "Concerning the Theory of Impact Ionization in Semiconductors," *Sov.Phys.JETP*, vol. 21, pp. 1135–1144, 1965.
35. T. Grasser, H. Kosina, C. Heitzinger, and S. Selberherr, "Accurate Impact Ionization Model which Accounts for Hot and Cold Carrier Populations," *Appl.Phys.Lett.*, vol. 80, no. 4, pp. 613–615, 2002.